3-28-2023

Concomitant inhibition of PPARγ and mTORC1 induces the differentiation of human monocytes into highly immunogenic dendritic cells.

Fernando Erra Diaz

Ignacio Mazzitelli

Lucía Bleichmar

Claudia Melucci

Asa Thibodeau

See next page for additional authors

Authors

Fernando Erra Diaz, Ignacio Mazzitelli, Lucía Bleichmar, Claudia Melucci, Asa Thibodeau, Tomás Dalotto Moreno, Radu Marches, Gabriel A Rabinovich, Duygu Ucar, and Jorge Geffner

Cell Reports

Article

Concomitant inhibition of PPARγ and mTORC1 induces the differentiation of human monocytes into highly immunogenic dendritic cells

Graphical abstract

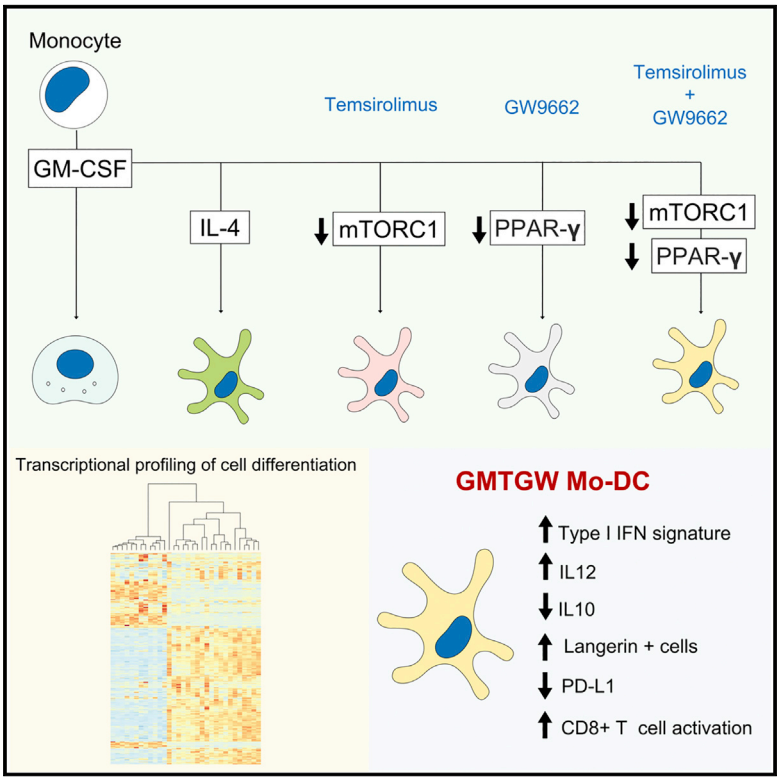

Authors

Fernando Erra Diaz, Ignacio Mazzitelli, Lucía Bleichmar, ..., Gabriel A. Rabinovich, Duygu Ucar, Jorge Geffner

Correspondence

duygu.ucar@jax.org (D.U.), jorgegeffner@gmail.com (J.G.)

In brief

Erra Díaz et al. show that pharmacological inhibition of PPARγ or mTORC1 promotes differentiation of GM-CSF-treated human monocytes into Mo-DCs. Moreover, the authors show that concomitant inhibition of mTORC1 and PPARγ induces differentiation of Mo-DCs with a strong phenotypic stability and a high capacity to expand antigen-specific $CD8^+$ T cells.

Highlights

- PPARγ or mTORC1 inhibitors turn GM-CSF into a Mo-DC differentiation inducer
- This differentiation process shows a distinctive transcriptional signature
- Concomitant mTORC1 and PPARγ inhibition promote a highly stable Mo-DC phenotype
- These Mo-DCs display a strong immunogenic profile

Erra Diaz et al., 2023, Cell Reports *42*, 112156
March 28, 2023
https://doi.org/10.1016/j.celrep.2023.112156

CellPress

Cell Reports

CellPress
OPEN ACCESS

Article

Concomitant inhibition of PPARγ and mTORC1 induces the differentiation of human monocytes into highly immunogenic dendritic cells

Fernando Erra Diaz,[1] Ignacio Mazzitelli,[1] Lucía Bleichmar,[1] Claudia Melucci,[1] Asa Thibodeau,[2] Tomás Dalotto Moreno,[3] Radu Marches,[2] Gabriel A. Rabinovich,[3,4] Duygu Ucar,[5,6,7,*] and Jorge Geffner[1,8,*]

[1]Facultad de Medicina, Instituto de Investigaciones Biomédicas en Retrovirus y SIDA, Universidad de Buenos Aires, CONICET, Buenos Aires, Argentina
[2]The Jackson Laboratory for Genomic Medicine, Farmington, CT 06032, USA
[3]Laboratorio de Glicomedicina, Instituto de Biología y Medicina Experimental (IBYME-CONICET), Buenos Aires, Argentina
[4]Facultad de Ciencias Exactas y Naturales, Universidad de Buenos Aires, Buenos Aires, Argentina
[5]The Jackson Laboratory for Genomic Medicine, Farmington, CT 06032, USA
[6]Department of Genetics and Genome Sciences, University of Connecticut Health Center, Farmington, CT 06030, USA
[7]Institute for Systems Genomics, University of Connecticut Health Center, Farmington, CT 06030, USA
[8]Lead contact
*Correspondence: duygu.ucar@jax.org (D.U.), jorgegeffner@gmail.com (J.G.)
https://doi.org/10.1016/j.celrep.2023.112156

SUMMARY

Monocytes can differentiate into macrophages (Mo-Macs) or dendritic cells (Mo-DCs). The cytokine granulocyte-macrophage colony-stimulating factor (GM-CSF) induces the differentiation of monocytes into Mo-Macs, while the combination of GM-CSF/interleukin (IL)-4 is widely used to generate Mo-DCs for clinical applications and to study human DC biology. Here, we report that pharmacological inhibition of the nuclear receptor peroxisome proliferator-activated receptor gamma (PPARγ) in the presence of GM-CSF and the absence of IL-4 induces monocyte differentiation into Mo-DCs. Remarkably, we find that simultaneous inhibition of PPARγ and the nutrient sensor mammalian target of rapamycin complex 1 (mTORC1) induces the differentiation of Mo-DCs with stronger phenotypic stability, superior immunogenicity, and a transcriptional profile characterized by a strong type I interferon (IFN) signature, a lower expression of a large set of tolerogenic genes, and the differential expression of several transcription factors compared with GM-CSF/IL-4 Mo-DCs. Our findings uncover a pathway that tailors Mo-DC differentiation with potential implications in the fields of DC vaccination and cancer immunotherapy.

INTRODUCTION

Dendritic cells (DCs) comprise a heterogeneous population of antigen-presenting cells that play critical roles in orchestrating the adaptive immune response.[1–3] They display the unique ability among antigen-presenting cells to activate naïve T cells, guiding their differentiation into different functional profiles.[4] Both in mice and humans, distinct populations of DCs have been described, differing in their location, function, phenotype, and origin.[5] The majority of DCs that populate the tissues in the absence of inflammation arise from the differentiation of specific myeloid hematopoietic precursors.[6] In contrast, DCs that infiltrate inflamed tissues mostly derive from the local differentiation of recruited monocytes.[7–11]

Monocytes are highly plastic cells able to differentiate into either macrophages (Mo-Macs) or DCs (Mo-DCs).[2] However, little is known about the factors that govern this cell-fate decision. In recent years, it has become clear that the nutritional status of immune cells and their metabolic adaptations play an important role in regulating their phenotype and function.[12] In this regard, we have previously reported that pharmacological inhibition of the nutrient sensor mammalian target of rapamycin complex 1 (mTORC1)[13] promotes monocyte differentiation into Mo-DCs, inhibiting their differentiation into Mo-Macs.[14] Accordingly, it has recently been reported that a Toll-like receptor (TLR)-mTORC1-dependent pathway promotes monocyte differentiation into Mo-Macs.[15]

Here, we investigated whether the peroxisome proliferator-activated receptor gamma (PPARγ) might be able to regulate monocyte fate decisions. The transcription factor PPARγ acts as a master regulator of adipogenesis and plays an important role in nutrient sensing, the regulation of lipid transport and metabolism, and the control of energy homeostasis.[16–18] Moreover, PPARγ has been shown to promote polarization of macrophages toward an M2 phenotype[19] and to inhibit CD4 T cell differentiation into T-helper (Th) 1 and Th17 profiles favoring differentiation of Foxp3$^+$ regulatory T cells (Tregs).[20–22] Early *in vitro* studies revealed that PPARγ expression is upregulated at the early steps of Mo-DC differentiation, suggesting that it might play a role in this process.[23] However, by re-analyzing

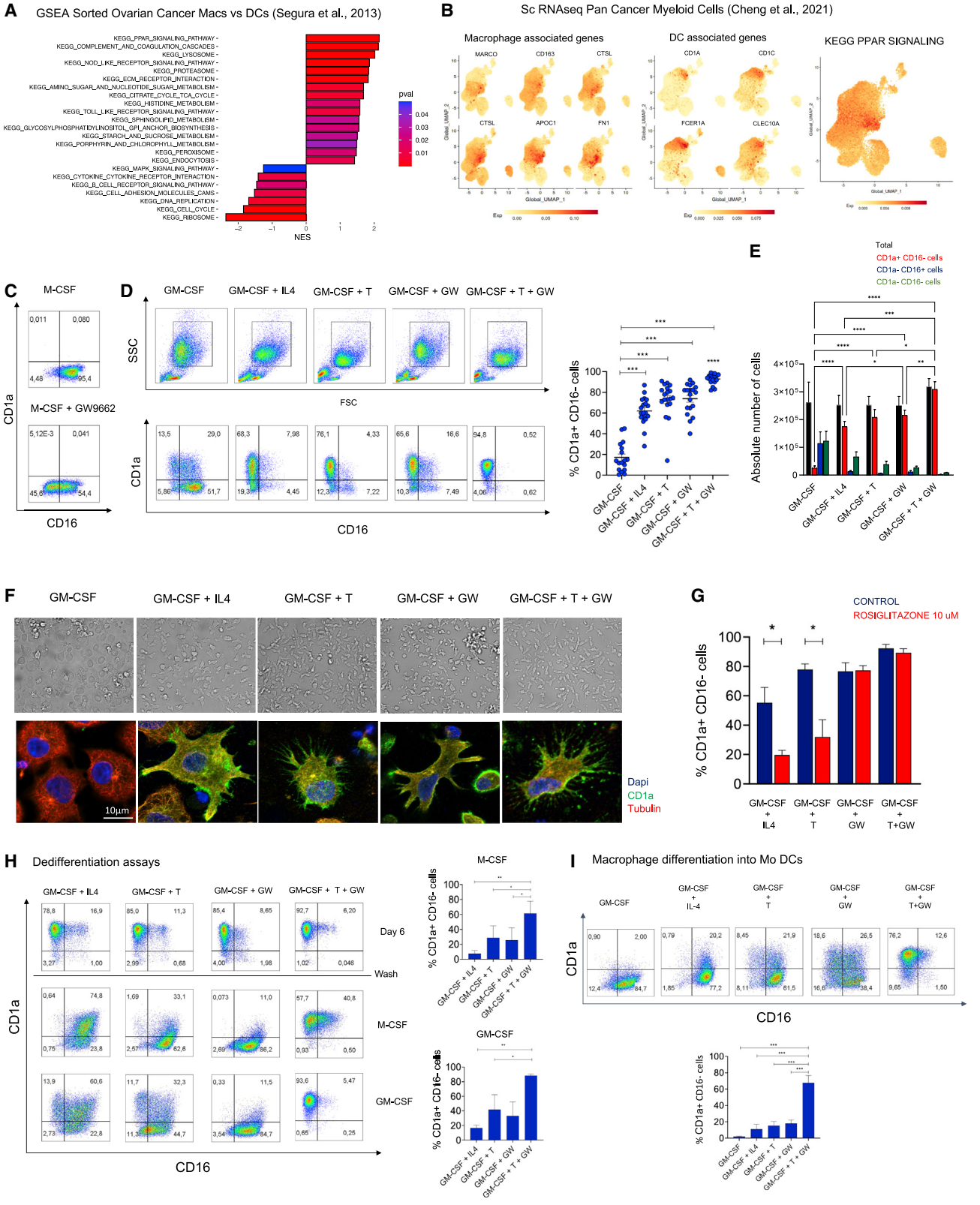

(legend on next page)

public gene expression data of human tumor-associated myeloid cells, we found that macrophages are markedly enriched in genes involved in PPARγ signaling compared with DCs. Here, we report that pharmacological inhibition of PPARγ turns GM-CSF into a strong inducer of Mo-DC differentiation. Moreover, we show that simultaneous blockade of PPARγ and mTORC1 promotes the differentiation of Mo-DCs with a remarkable phenotypic stability, a strong immunogenic profile, and a particular transcriptional signature.

RESULTS

PPARγ inhibition turns GM-CSF into a strong inducer of Mo-DC differentiation

Studies performed in mice have previously shown that a large fraction of tumor-associated macrophages are monocyte derived.[24,25] Moreover, according to data from mice and human studies, it appears that a significant fraction of tumor-associated DCs arise from the local differentiation of infiltrating monocytes.[8,26,27] To gain insight into the pathways involved in Mo-Macs and Mo-DCs differentiation *in vivo*, we investigated the transcriptional signatures of tumor-associated macrophages (TAMs) and DCs by re-analyzing published datasets. Gene set enrichment analysis (GSEA) of macrophages and DCs from ovarian cancer ascites[27] revealed that genes associated with PPAR signaling pathways showed the highest enrichment score in macrophages compared with DCs (Figure 1A; Table S1). PPARs comprise a family of transcription factors that play a central role in lipid metabolism and energy homeostasis.[28] Among the leading-edge genes (Table S1), we found that many of them were specifically associated with PPARγ signaling, including *FABP4*, *FABP3*, *LPL*, *CD36*, and *PPARG*[16] (Figure S1A). To further evaluate whether this enrichment actually represented a common signature in different tumors, single-cell RNA sequencing (scRNA-seq) data of tumor-infiltrating myeloid cells from 15 different types of cancer were analyzed.[29] An increased expression of PPARγ-associated genes in TAMs compared with DCs was also observed (Figures 1B, S1B, and S1C). Overall, these observations suggest that activation of PPARγ could promote the differentiation of infiltrating monocytes into macrophages in the tumor environment. We then analyzed whether *in vitro* differentiation of monocytes into Mo-Macs and Mo-DCs was also associated with differential expression of PPARγ-associated genes. By re-analyzing published datasets from Sander and coworkers,[30] we found that, after 3 days of culture with GM-CSF, monocyte-derived cells displayed a higher expression of PPARγ-associated genes compared with monocytes cultured with GM-CSF plus IL-4, the traditional strategy to obtain monocyte-derived DCs[31] (Figure S1D; Table S2). Supporting an important role of PPARγ in the differentiation of monocytes into Mo-Macs, it has been reported that lysophosphatidic acid induces the differentiation of monocytes into macrophages through a PPARγ-dependent pathway in both mice and humans.[32]

Considering the higher expression of PPARγ-associated genes in macrophages compared with DCs, we hypothesized that PPARγ inhibition might promote monocyte differentiation into DCs. To test this hypothesis, we used the PPARγ antagonist GW9662 and the PPARγ agonist rosiglitazone. As expected, rosiglitazone induced the expression of the PPARγ reporter gene *FABP4*,[33] while GW9662 markedly inhibited this response (Figure S2A). The impact of PPARγ on the differentiation of monocytes into Mo-Macs or Mo-DCs was analyzed by determining the expression of CD1a and CD16[27,34] in monocytes cultured with either macrophage colony-stimulating factor (M-CSF) or GM-CSF, two cytokines that drive monocyte differentiation into

Figure 1. PPARγ inhibition in human monocytes turns GM-CSF into a strong inducer of Mo-DC differentiation

(A) Gene set enrichment analysis (GSEA) was performed using microarray data (GSE40484, Segura et al., 2013) from sorted myeloid cells obtained from ascitic fluid of ovarian cancer patients. $CD11c^{++}$ $HLA\text{-}DR^{++}$ $CD16^{+}$ $CD1a^{-}$ cells (Mo-Macs) and $CD11c^{++}$ $HLA\text{-}DR^{++}$ $CD16^{-}$ $CD1a^{+}$ cells (Mo-DCs) were compared. Pathways were obtained from the Kyoto Encyclopedia of Genes and Genomes (KEGG) database. Pathways with $p < 0.05$ are presented in the comparison between both groups.

(B) UMAPs showing the expression profile of scRNA seq data of tumor-infiltrating myeloid cells, analyzed using the online database and Web platform (http://panmyeloid.cancer-pku.cn). The combined downsampled dataset of myeloid cells found in 15 different cancer types is presented. Typical macrophage and DC-associated genes highlight macrophage and DC populations. The expression of the PPAR signaling module from KEGG is shown in the right panel (geometric mean).

(C) Human monocytes (1×10^6/mL) were cultured for 6 days in the presence of M-CSF (100 ng/mL) with or without the addition of GW9662 (10 μM). The expression of CD1a and CD16 was then analyzed by FACS. A representative experiment is shown.

(D–F) Monocytes (1×10^6/mL) were cultured for 6 days in the presence of GM-CSF (50 ng/mL) with or without IL-4 (30 ng/mL), temsirolimus (50 nM), GW9662 (10 μM), or the combination of GW9662 (10 μM) + temsirolimus (50 nM). The expression of CD16 and CD1a was then analyzed by FACS. Representative dot plots and the results from 18 different experiments are shown in (D). Absolute cell counts for the different populations are presented in (E). Cell morphology was analyzed by brightfield (upper) and confocal microscopy (lower) (F).

(G) Monocytes (1×10^6/mL) were cultured for 6 days in the presence of GM-CSF (50 ng/mL) in the absence or presence of IL-4 (30 ng/mL), temsirolimus (50 nM), GW9662 (10 μM) or the combination of GW9662 (10 μM) and temsirolimus (50 nM), with or without rosiglitazone (10 μM). The expression of CD1a and CD16 was then analyzed by FACS ($n = 4$).

(H) Monocytes were cultured as described in (D). After 6 days, cells were washed and cultured for an additional period of 6 days in the presence of M-CSF (100 ng/mL) or GM-CSF (50 ng/mL). Then, the expression of CD1a and CD16 was analyzed by FACS. Representative dot plots and bar plots from four different experiments are shown.

(I) Monocytes (1×10^6/mL) were cultured for 7 days in the presence of M-CSF (100 ng/mL) in order to induce their differentiation into Mo-Macs. Cells were then washed and cultured for 6 days in the presence of GM-CSF (50 ng/mL), GM-CSF + IL-4 (30 ng/mL), GM-CSF + temsirolimus (50 nM), GM-CSF + GW9662 (10 μM), or GM-CSF + GW9662 (10 μM) + temsirolimus (50 nM). The expression of CD1a and CD16 was then analyzed by FACS. Representative dot plots are presented in the upper panel and bar plots from six different experiments are shown in the lower panel. Representative experiments or the mean ± SEM of n different donors are shown. *$p < 0.05$, **$p < 0.001$, and ***$p < 0.0001$. ****$p < 0.001$ versus all other conditions.

macrophage-like cells.[35] Moreover, based on our previous findings showing that mTORC1 inhibition promotes Mo-DC differentiation in the presence of GM-CSF,[14] we also evaluated the effect of PPARγ inhibition on Mo-DC differentiation induced by GM-CSF plus the mTORC1 inhibitor temsirolimus. As expected, mTORC1 activity was markedly inhibited by temsirolimus, while it remained unaffected by GW9662 (Figure S2B). Blocking PPARγ with GW9662 did not affect M-CSF's ability to induce monocyte differentiation into Mo-Macs (Figure 1C), although it induced the downregulation of CD16 expression (Figure S2C). In contrast, we found that the PPARγ inhibitor GW9662, but not the PPARα and PPARδ inhibitors GW6471 and GSK3787, switched the biological activity of GM-CSF from a macrophage differentiation factor toward a DC differentiation factor (Figures 1D and S2D and S2E). Interestingly, culturing monocytes with GM-CSF in the presence of both the mTORC1 inhibitor temsirolimus and GW9662 (GMTGW Mo-DCs) provided the highest yields of $CD1a^+$ $CD16^-$ cells (Figures 1D and 1E). It has been reported that human monocytes cultured with GM-CSF display some proliferative capacity.[36] In agreement with this observation, we found that GM-CSF promoted the proliferation of a fraction of monocytes. By contrast, no proliferation was observed in the course of Mo-DC differentiation, irrespective of the stimuli used (Figure S2F). As expected, GM Mo-Macs display typical macrophage-like features, while GMIL4 Mo-DCs, GMT Mo-DCs, GMGW Mo-DCs, and GMTGW Mo-DCs showed a characteristic DC morphology together with a high surface expression of CD1a (Figure 1F) (Video S1).

In addition to the established method to obtain Mo-DCs based on the use of GM-CSF and IL-4, it has been shown that monocyte treatment with M-CSF, interleukin (IL)-4, and tumor necrosis factor alpha (TNF-α) yields a mixture of inflammatory macrophages and DCs.[34] Having shown that PPARγ inhibition enabled GM-CSF to induce the differentiation of Mo-DCs, we then analyzed whether it further promoted the differentiation of Mo-DCs induced by either GM-CSF/IL-4 or M-CSF/IL-4/TNF-α. No promotion of Mo-DC differentiation was observed (Figure S2G). Additionally, we analyzed the effect of the PPARγ agonist rosiglitazone on Mo-DC differentiation. Rosiglitazone strongly inhibited both GMIL4 Mo-DCs and GMT Mo-DCs differentiation. As expected, rosiglitazone did not exert any inhibitory effect on cells treated with GW9662; i.e., GMGW Mo-DCs and GMTGW Mo-DCs (Figures 1G and S2H). To analyze whether the promotion of Mo-DC differentiation in GM-CSF-treated monocytes induced by IL-4 or the mTORC1 inhibitor temsirolimus might be related to an inhibition of PPARγ-dependent pathways, we also determined the expression of the PPARγ reporter gene FABP4 induced by rosiglitazone. Neither IL-4 nor temsirolimus exerted any inhibitory effect (Figure S2I).

The phenotypic stability of DCs and the ability of GW9662 to promote the differentiation of fully differentiated macrophages into DCs were then assessed. To analyze the phenotypic stability of Mo-DCs, already differentiated DCs were washed and cultured for an additional period of 6 days in the presence of M-CSF or GM-CSF, and cell phenotype was evaluated. A marked reduction in the expression of CD1a together with an increased expression of CD16, indicative of a dedifferentiation process, was observed for GMIL4 Mo-DCs, GMT Mo-DCs, and GMGW Mo-DCs, but not for GMTGW Mo-DCs (Figure 1H). Afterward, we investigated whether Mo-Macs could be differentiated into Mo-DCs. *In vitro* experiments have shown that Mo-Macs have limited plasticity to become Mo-DCs when treated with GM-CSF + IL4.[37] In these experiments, monocytes were differentiated into macrophages by culturing them for 6 days with M-CSF. Cells were then washed and cultured with GM-CSF, GM-CSF/IL-4, GM-CSF/temsirolimus, GM-CSF/GW9662, or GM-CSF/temsirolimus/GW9662 for an additional period of 6 days, and cell phenotype was analyzed by flow cytometry. Only the combination GM-CSF/temsirolimus/GW9662 efficiently promoted the differentiation of Mo-Macs into DCs (Figure 1I). We conclude that simultaneous inhibition of PPARγ and mTORC1, in the context of GM-CSF stimulation, not only yields Mo-DCs with a stable phenotype but also enables the efficient differentiation of Mo-Macs into DCs.

Additionally, we investigated whether transient exposure to temsirolimus and GW9662 was enough to promote the differentiation of Mo-DCs. Probably reflecting the irreversible action of both drugs on their pharmacological targets,[38] we observed that monocytes exposed to these drugs for only 1 h followed by extensive washing were effectively conditioned to become DCs, after culturing them for 6 days with GM-CSF (Figure S3A). PGE2 is an important lipid mediator known to inhibit GM-CSF/IL-4-induced Mo-DC differentiation, promoting the generation of M2-like macrophages.[39] In contrast with the observations made in GM-CSF/IL-4-induced Mo-DC differentiation, PGE2 was completely unable to inhibit the differentiation of either GMT Mo-DCs, GMGW Mo-DCs, or GMTGW Mo-DCs (Figure S3B). Finally, we explored whether temsirolimus and GW9662 were also able to induce the differentiation of DCs in a more complex scenario. In these experiments, whole peripheral blood mononuclear cells (PBMCs) were stimulated by anti-CD3/anti-CD8-coated beads in the absence or presence of temsirolimus and GW9662, and cells were cultured for 6 days without the addition of exogenous GM-CSF. Then, the phenotype of $MHCII^+$ cells within the monocyte/macrophage gate of the forward scatter/side scatter (FSC/SSC) dot plot was analyzed. We found that temsirolimus and/or GW9662 promoted the differentiation of a population of $CD1a^+$ $CD16^-$ DCs (Figure S3C).

Simultaneous inhibition of PPARγ and mTORC1 enables GM-CSF to direct Mo-DC differentiation, leading to Th1 polarization and robust $CD8^+$ T cell activation

The functional status of Mo-DCs obtained under different experimental conditions was analyzed. As expected, GM Mo-Macs showed only a modest upregulation of both CD86 and major histocompatibility complex (MHC) class II molecules upon lipopolysaccharide (LPS) stimulation. By contrast, all Mo-DC populations assessed showed a clear upregulation of these maturation markers, with no differences observed among them (Figures 2A and S4A). Afterward, the production of cytokines induced by LPS was evaluated. Interestingly, GMTGW Mo-DCs showed a particular signature characterized by the highest IL-12 production and undetectable IL-10 release (Figure 2B). Consistent with this cytokine profile, this DC population induced the highest production of Th1-type cytokines including interferon (IFN)-γ, IL-2, and TNF-α, in the course of the mixed lymphocyte reactions (Figures 2C and 2D).

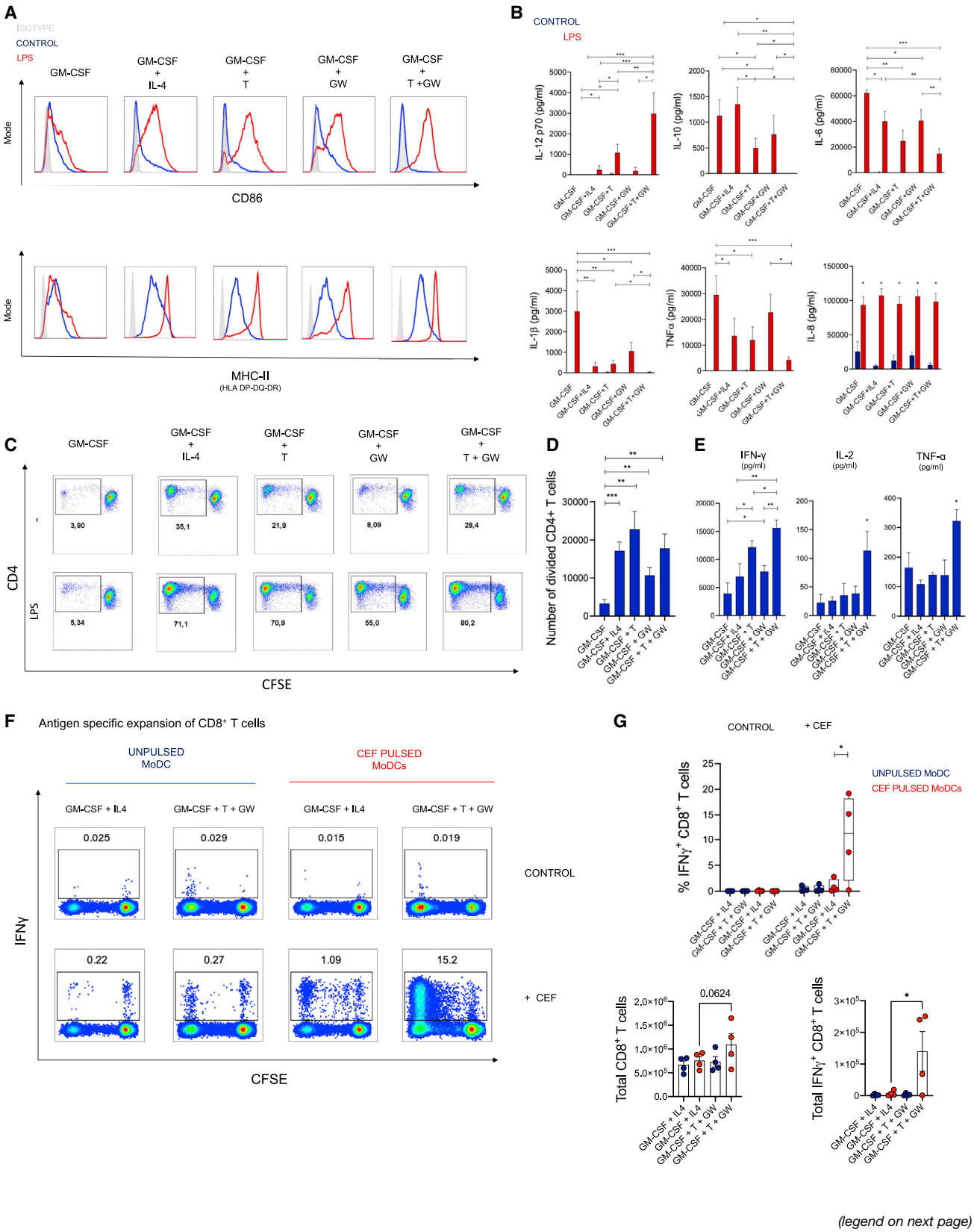

(legend on next page)

Two additional functions were evaluated: phagocytosis and antigen processing. Phagocytosis was assessed using zymosan particles labeled with a pH-sensitive fluorescent dye (pHRodo), allowing to distinguish endocytosed particles located in acidic endosomal compartments from those attached to the cell surface. No differences in the phagocytic activity were observed among the different Mo-DCs evaluated (Figure S4B). A similar ability to process endocytosed antigens was also observed by evaluating OVA-DQ degradation revealed as an increased fluorescence emission (Figure S4C).

Finally, the ability of Mo-DCs to induce the expansion of $CD8^+$ T cells in an antigen-dependent manner was analyzed. To avoid unspecific activation of T cells by fetal calf serum proteins, these experiments were performed with human AB^+ serum collected after a 12-h fasting period. Mo-DCs used in these experiments were also generated in the presence of human AB^+ serum, obtaining similar yields of $CD1a^+$ CD16− cells compared with those cultures performed in culture medium supplemented with fetal calf serum (Figure S4D). The protocol used to analyze the activation of $CD8^+$ T cells and the gating strategy are summarized in Figures S5A and S5B, respectively. Briefly, GMIL4 Mo-DCs and GMTGW Mo-DCs were pulsed, or not, with a CEF peptide pool (10 μg/mL) including 32 MHC class I-restricted viral peptides from cytomegalovirus (CMV), Epstein-Barr virus (EBV), and influenza virus. DCs were then cocultured for 12 days with autologous 5,6-carboxyfluorescein diacetate succinimidyl ester (CFSE)-labeled PBMCs using a Mo-DC:PBMC ratio of 1:2. Half of the culture medium was changed to fresh medium at days 6 and 9, but no other factors were introduced into the system. After 12 days, cells were re-exposed, or not, to CEF peptides in the presence of autologous PBMCs used as antigen-presenting cells, and the frequency of antigen-specific $CD8^+$ T cells was analyzed by fluorescence-activated cell sorting (FACS), by studying IFN-γ production. Interestingly, we found that GMTGW Mo-DCs induced a much stronger expansion of antigen-specific $CD8^+$ T cells compared with GMIL4 Mo-DCs (Figures 2F and 2G).

Early transcriptional programs triggered by simultaneous mTORC1/PPAR-γ blockade or IL-4 in GM-CSF-treated monocytes

RNA sequencing (RNA-seq) data were generated to analyze the transcriptional signature of Mo-DCs both at the beginning (8 h) and at the end of the differentiation process (6 days). Gene expression can be interactively accessed at https://ferra-uba-jax.shinyapps.io/shinnyapp/. Hierarchical clustering of the top 500 highly variable genes observed at 8 h of culture showed that treatment with GM-CSF and IL-4 markedly differed from the other experimental conditions (GM-CSF/temsirolimus, GM-CSF/GW9662, or GM-CSF/temsirolimus/GW9662), each of them displaying both shared and specific gene expression patterns (Figure 3A). To study the specific transcriptional changes induced by IL-4, temsirolimus, GW9662, or the combination temsirolimus/GW9662 at 8 h of culture, we performed a differential expression analysis for each experimental condition versus monocytes cultured only in the presence of GM-CSF (Table S3). Distinct early transcriptional profiles were observed among the different treatments (Figures 3B and S6A). Top upregulated and downregulated genes were specific to each experimental condition (Figure 3C). For example, IL-4 induced the expression of *ALOX15* and *FABP4*, two top IL-4-regulated genes,[30,40,41] while temsirolimus upregulated the expression of *SECTM1*, a costimulatory ligand for T and natural killer (NK) cells,[42] together with the Wnt signaling modulator *FRAT1*, the purinergic receptor *P2RY13*, and the transcriptional regulator of SIRT1, *FOXQ1*.[43] On the other hand, temsirolimus downregulated the expression of *FABP4* and *FABP5*, two PPARγ targets.[16,44] The compound GW9662 induced the expression of the *IL24* gene, a poorly characterized cytokine that exerts a direct cytotoxic effect on melanoma cells[45] together with *CLDN1* (Claudin-1), *FFAR4* (free fatty acid receptor 4), *EPGN* (epithelial mitogen), *AREG* (amphiregulin, a member of the epidermal growth factor family), and *TNFSF18* (TNF superfamily member 18), a costimulator that lowers the threshold for T cell activation. Genes downregulated by GW9662 included *FBP1* and *CD1D*, two genes known to be regulated by PPARγ,[46,47] together with *FN1* (fibronectin 1), a promoter of M2-like macrophage polarization[35]; *GDF15* (growth differentiation factor 15), a cytokine that inhibits DC maturation and IL-12 production[48]; and *WNT5A*, a non-canonical WNT ligand able to inhibit the differentiation of Mo-DCs and to promote the induction of a tolerogenic phenotype.[49,50] As expected, monocytes treated with temsirolimus plus GW9662 shared a number of features with cells treated individually with temsirolimus or GW9662, such as an increased expression of *IL24*, *CLDN1*, *FOXQ1*, and *SECTM1*,

Figure 2. Simultaneous inhibition of PPAR-γ and mTORC1 in human monocytes enables GM-CSF to induce the differentiation of immunogenic Mo-DCs

(A and B) Monocytes (1×10^6/mL) were cultured for 6 days with GM-CSF (50 ng/mL) in the absence or presence of IL-4 (30 ng/mL), temsirolimus (50 nM), GW9662 (10 μM), or the combination of GW9662 (10 μM) + temsirolimus (50 nM). Afterward, cells were washed and cultured for 18 h in the presence or absence of LPS (10 ng/mL). Then, the expression of CD86 and MHCII molecules and the concentrations of cytokines in cell supernatants (IL12p70, IL-10, IL-6, IL-1β, TNFα, and IL-8) were measured (n = 6).

(C–E) Mo-Macs and Mo-DCs were obtained as described above, and mixed lymphocyte cultures (MLRs) were performed using a $CD4^+$ T cell/antigen-presenting cell ratio of 4:1. In (C), $CD4^+$ T cell proliferation was measured by CFSE dilution. In (D), the absolute number of proliferating $CD4^+$ T cells is shown. In (E), the concentration of cytokines in the supernatants of MLRs is shown.

(F and G) Monocytes were cultured for 6 days in RPMI medium supplemented with 7% heat-inactivated human AB serum, in the presence of GM-CSF (50 ng/mL) + IL-4 (30 ng/mL) or GM-CSF (50 ng/mL) + temsirolimus (50 nM) + GW9662 (10 μM), to induce Mo-DC differentiation. Cells were then washed and cultured for 18 h in the presence of LPS (10 ng/mL) with or without the addition of CEF peptide pool (10 μg/mL). Antigen pulsed and unpulsed Mo-DCs were washed and cocultured with autologous CFSE-labeled PBMCs for 12 days at a 1:2 ratio. The proportion of CEF-reactive $CD8^+$ T cells was then assessed by intracellular staining and FACS by evaluating IFN-γ production, after re-exposure of cells to the CEF peptide pool (1 μg/mL) (F and G). Absolute numbers of total CD8 T cells (G, bottom left) and CEF-reactive CD8 T cells (G, bottom right) are shown. Representative experiments or the mean ± SEM of n different donors (A–E, n = 6, and G, n = 4) are shown. *$p < 0.05$, **$p < 0.001$, and ***$p < 0.0001$.

CellPress
OPEN ACCESS

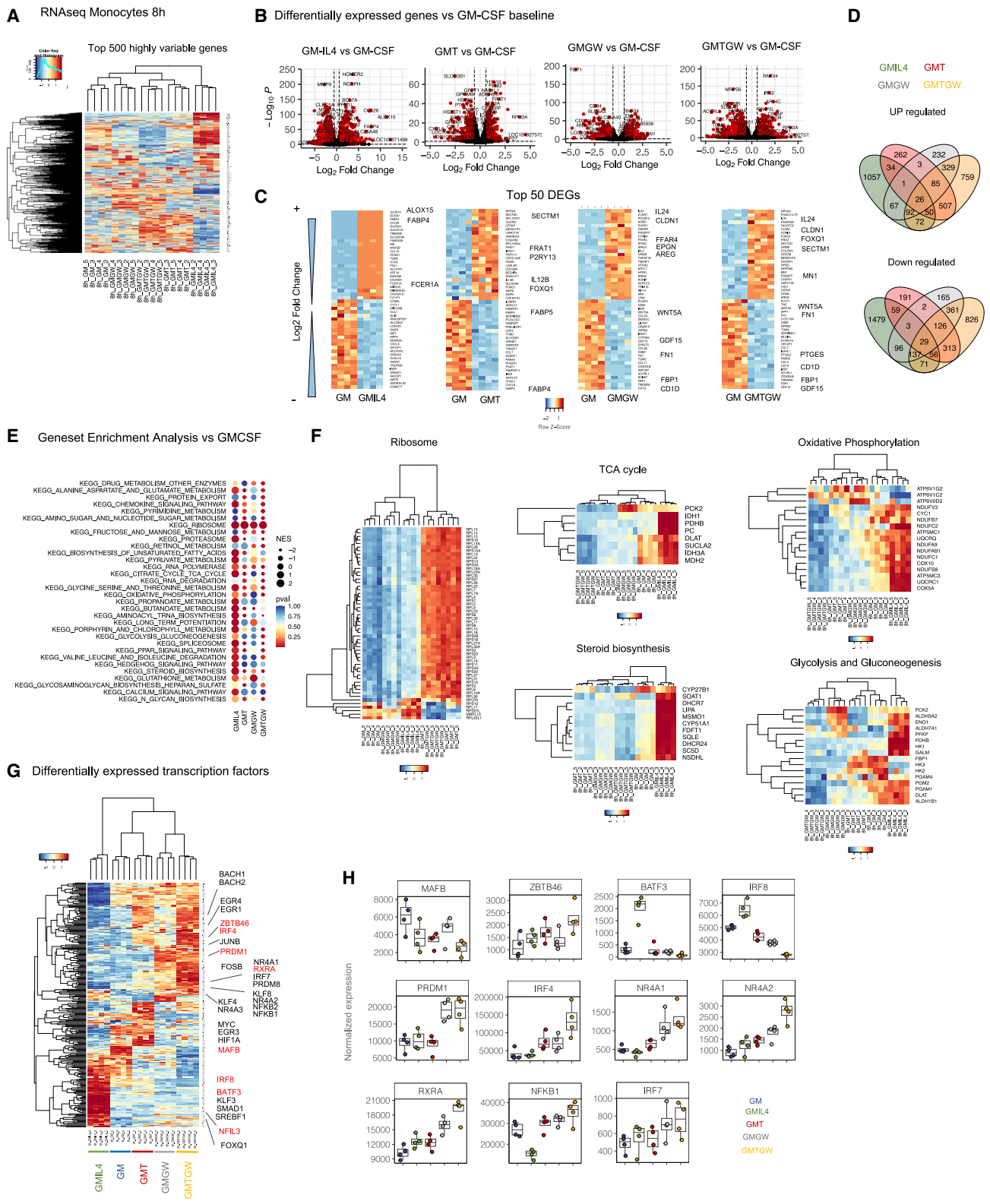

(legend on next page)

and a reduced expression of *FN1*, *FBP1*, and *CD1D*. (Figures 3C and S6B). Not only did IL-4 induce a very distinct transcriptional signature compared with the other treatments but also the combination of temsirolimus plus GW9662 modulated a large set of genes that were not significantly affected in cells treated individually with temsirolimus or GW9662 (Figures 3D and S6A; Table S3). Moreover, beyond the major differences observed between the early transcriptomic profile of IL-4 versus temsirolimus plus GW9662-treated monocytes, they shared some transcriptional features; 240 upregulated and 293 downregulated genes. As expected, among the shared downregulated genes were those associated with a macrophage-like profile, such as *MMP9*, *MARCO*, *GPR84*, *MAFB*, and *CD14* (Figure S6C).

GSEA comparing each experimental condition with GM-CSF-treated monocytes was performed, and gene sets that showed statistically significant enrichments in at least one comparison were analyzed (Figure 3E; Table S3). Surprisingly, all the experimental treatments leading to Mo-DC differentiation displayed an increased expression of genes associated with ribosome structure and function (Figures 3E, 3F, and S6D). Tricarboxylic acid (TCA) cycle, steroid biosynthesis, and PPAR signaling-associated genes were significantly induced in monocytes treated with GM-CSF and IL-4. Conversely, these gene sets were downregulated by temsirolimus and mildly inhibited by GW9662, defining a sharp contrast in the early transcriptional features of these groups compared with the GMIL4 group. Interestingly, analysis of the genes that showed significant changes among comparisons revealed that the combination of temsirolimus and GW9662 exerted an additive effect on some of these genes. This was particularly evident in the case of the TCA cycle genes *IDH3A* (isocitrate dehydrogenase) and *MDH2* (malate dehydrogenase) as well as in a number of genes involved in the mitochondrial respiratory chain (*CYC1*, *COX10A*, *COX5A*, *NDUFA9*, *NDUFAB1*, *NDUFAB7*, *NDUFC1*, *UQCRC1*, and *UQCRQ*) (Figures 3F and S7A). Moreover, because PPARγ-dependent pathways are involved in lipid uptake,[51] we measured the uptake of fluorescently labeled palmitic acid (BodipyFLC16) in monocytes previously treated for 18 h with GM-CSF in the presence of IL-4, GW9662, temsirolimus, or GW9662 and temsirolimus. The uptake of fluorescently labeled palmitic acid (BodipyFLC16) was significantly reduced in cells cultured with temsirolimus or GW9662 and further decreased when both treatments were combined (Figure S7B).

Since early changes in the expression of transcription factors are crucial to define cell identity in the context of cell differentiation, an analysis of their differential expression among the distinct treatments was conducted. A sharp contrast was observed between the changes induced by GMIL4 versus GMTGW (Figures 3G and 3H; Table S3). IL-4 upregulated the expression of *BATF3* and *IRF8* genes, both associated predominantly with cDC1 differentiation, while temsirolimus plus GW9662 induced the expression of *IRF4* and *PRDM1* (Blimp1), two transcription factors involved in cDC2 and Mo-DC commitment.[34,52] Interestingly, the changes induced in monocytes treated individually with temsirolimus or GW9662 showed important differences compared with those induced by temsirolimus plus GW9662, suggesting that the combined action of these two compounds could not be explained solely in terms of their individual behavior (Figure 3H; Table S3). Noticeably, we observed that the combination of GW9662 and temsirolimus induced the coordinated expression of a cluster of genes including those coding for the NR4A orphan nuclear receptors *NR4A1* and *NR4A2*,[53] which interact with the retinoid acid receptor alpha *RXRA*,[54] a gene that also showed the highest expression in monocytes treated with GW9662 and temsirolimus (Figure 3H).

Transcriptional signature of Mo-DCs differentiated with GM-CSF in the presence of IL-4 or mTORC1 and/or PPARγ inhibitors

To further explore the mechanisms underlying Mo-DC differentiation induced by mTORC1 and/or PPARγ inhibition and understand the molecular mechanisms implicated in stronger immunogenicity of these cells, bulk RNA-seq of sorted Mo-DCs ($CD1a^+$ $CD16^-$cells) was performed at the end of the differentiation process; i.e., at 6 days of culture (Table S4). Gene expression profiles observed at early time points (8 h of culture) are also shown for each treatment. Culture of monocytes with either GM-CSF/IL-4 or GM-CSF, and mTORC1 and/or PPARγ inhibitors led to the acquisition of a set of typical DC-associated genes (*CD1A*, *CD1C*, *CD1B*, *CD1E*, *CLEC10A*, *PARM1*, and *ZBTB46*) and a downregulated expression of macrophage-associated genes (*CD14*, *MERTK*, and *PPARG*). Moreover, we found that GMT Mo-DCs, GMGW Mo-DCs, and GMTGW Mo-DCs showed a significant expression of the Langerhans cell markers *CD207* (Langerin) and *CLDN1* (Claudin-1), while only GMIL4 Mo-DCs

Figure 3. A divergent early transcriptional signature is induced in GM-CSF-treated monocytes by IL-4 or by blockade of mTORC1 and/or PPAR-γ

(A) RNA-seq of human monocytes cultured for 8 h in the presence of GM-CSF (50 ng/mL), GM-CSF (50 ng/mL) + IL-4 (30 ng/mL), GM-CSF (50 ng/mL) + temsirolimus (50 nM), GM-CSF (50 ng/mL) + GW9662 (10 μM), or GM-CSF (50 ng/mL) + temsirolimus (50 nM) + GW9662 (10 μM). Top 500 highly variable genes of donor normalized z values are shown (n = 4 for each condition).

(B) Volcano plots show the results of differential expression analysis between each experimental condition compared with GM-CSF-treated cells. Differentially expressed genes (DEGs) are defined as FC > 1.5, adjusted p value <0.1.

(C) Heatmaps of the top 50 up- and downregulated DEGs in each comparison versus GM-CSF.

(D) Venn diagrams showing the intersections of up- and downregulated DEGs versus GM-CSF.

(E) GSEA versus GM-CSF-treated cells. Pathways showing a significant enrichment ($p < 0.05$) in at least one comparison are presented. Dot size reflects the normalized enrichment score (NES) versus GM-CSF, and color scale indicates p values.

(F) Donor normalized z values of genes included in the selected KEGG gene sets. Only DEGs (in at least one comparison) are presented in the heatmaps.

(G) Transcription factors were selected among DEGs versus GM-CSF in at least one comparison (n = 280). Heatmap and hierarchical clustering of donor normalized gene expression z values are presented.

(H) Normalized gene expression values of selected transcription factors.

CellPress
OPEN ACCESS

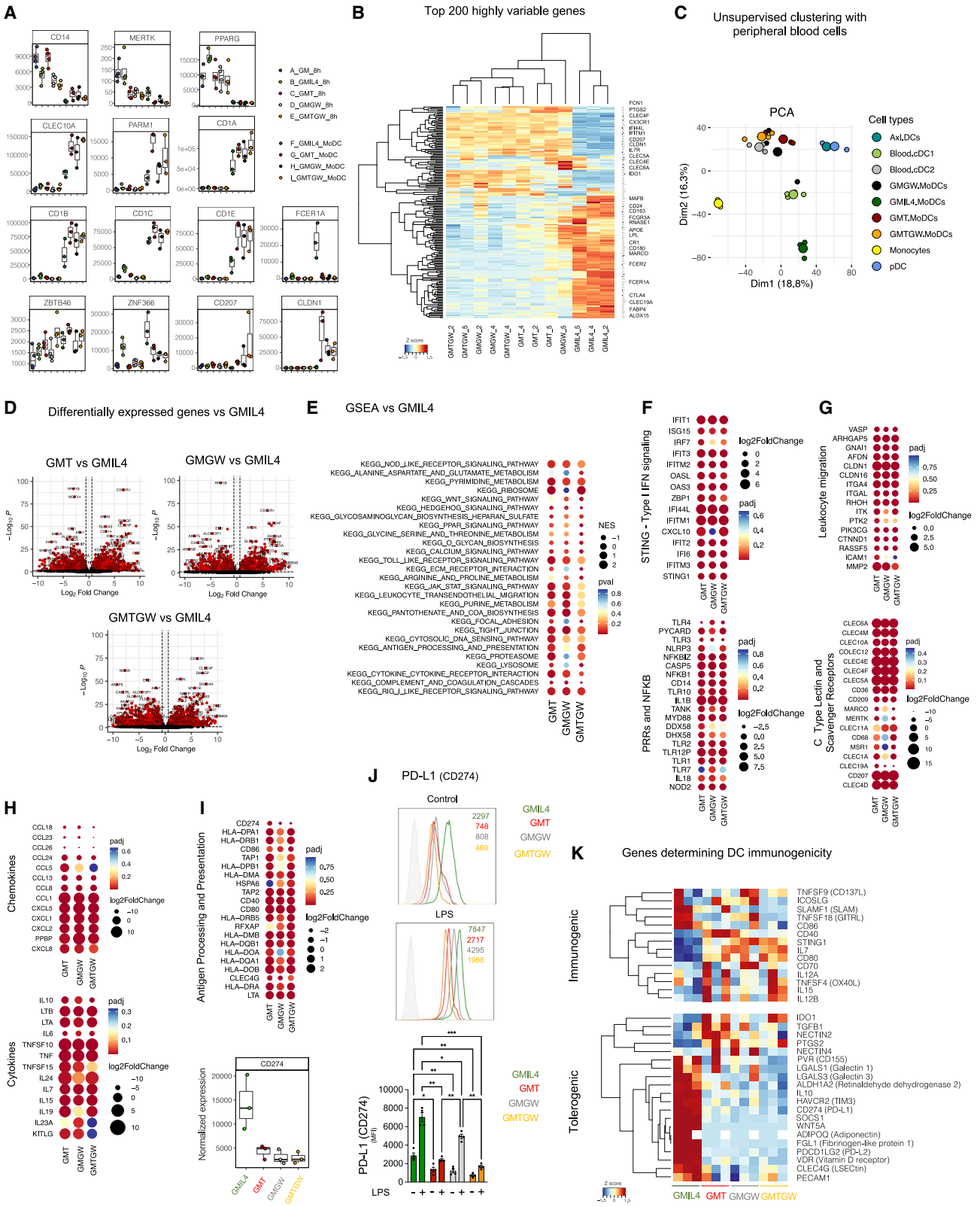

(legend on next page)

expressed the *FCER1A* (Fc epsilon receptor Ia) gene (Figure 4A). The expression of CD207 (Langerin) and FcεRI were validated by flow cytometry. GMT Mo-DCs and GMGW Mo-DCs were characterized by the presence of a subpopulation of Langerin$^+$ CD1a$^+$ cells, which was further increased in GMTGW Mo-DCs (Figure S8A). On the other hand, we observed that only GMIL4 Mo-DCs showed a significant expression of FcεRI (Figure S8B).

Analysis of the top 200 highly variable genes revealed not only that GMIL4 Mo-DCs display a very different transcriptomic profile compared with Mo-DCs obtained under the influence of mTORC1 or PPAR-γ inhibitors but also that these Mo-DCs shared a similar transcriptomic profile, characterized by an increased expression of genes coding for several C-type lectin receptors (*CLEC4F*, *CLEC5A*, *CLEC4E*, and *CLEC6A*); the enzyme *IDO1*, *IL7R*, *CX3CR1* (fractalkine receptor); and the type I interferon signature genes *IFI44L* and *IFITM1*. Conversely, GMIL4 Mo-DCs showed a higher expression of *CD24*; *CTLA4*; the PPARγ targets *FABP4*, *LPL*, and *APOE*; *CR1* (C3b/C4b receptor); and the macrophage-associated genes *MARCO* and *CD163* (Figure 4B). By using publicly available datasets, we then compared the transcriptomic profile of *in vitro*-generated Mo-DCs with the starting monocyte population as well as with cDC1 (CD141$^+$), cDC2 (CD1c$^+$), pDCs, and Axl$^+$ DCs. Principal-component analysis (PCA) (Figures 4C and S8C) revealed that all DC types clustered separately from freshly isolated monocytes. Interestingly, PCA also revealed that GMT, GMGW, and GMTGW Mo-DCs showed closer proximity with type 2 classical CD1c$^+$ blood DCs (Figures 4C and S8C), and shared a large fraction of differentially expressed genes (DEGs) compared with GMIL4 Mo-DCs (Figures 4D and S8D; Tables S4 and S5). Moreover, considering that GMIL4 Mo-DCs displayed a higher expression of several macrophage-associated genes, by using publicly available datasets, we also analyzed how the different types of *in vitro*-generated Mo-DCs clustered with TAMs and DCs found *in vivo* (Figure S8E; Table S5). PCA revealed that GMT, GMGW, and GMTGW Mo-DCs clustered in closer proximity with tumor-associated DCs compared with GMIL4 Mo-DCs. Analysis of the top 100 genes that explained PC1 and PC2 revealed that GMIL4 Mo-DCs shared with TAMs a higher expression of typical macrophage-associated markers (*CD209*, *C2*, *MARCO*, *AQP9*, and *FABP4*). Conversely, GMT, GMGW, and GMTGW Mo-DCs displayed a higher expression of several DC-associated genes (*CD1B*, *CD1A*, *PARM1*, *CD1C*, and *CCR7*) in a fashion comparable with intratumoral DCs (Figure S8E).

As the timely coordinated expression of transcription factors is critical in defining and maintaining cell identity, we analyzed whether the same changes observed at earlier time points of differentiation (8 h) were also observed in differentiated Mo-DCs. As expected, we found major differences in the expression of transcription factors between 8 h and 6 days of culture for all Mo-DC populations (Figure S8F). Most of the transcription factors that were induced after 8 h of culture in monocytes treated with GM-CSF plus temsirolimus and/or GW9662 such as *NR4A2*, *NR4A1*, and *IRF4* were downregulated when analyzed at day 6. Despite this, some transcription factors, including *BACH1*, *IRF7*, and *NFKB1*, remained with a higher expression in GM-CSF plus temsirolimus and/or GW9662 Mo-DCs compared with GMIL4 Mo-DCs. By contrast, the expression of the cDC1-associated transcription factors induced by GM-CSF + IL-4, such as *BATF3*, *NFIL3*, and to a lesser extent *IRF8*, was sustained over time. Additionally, the transcription factor expression pattern of GMT, GMGW, and GMTGW Mo-DCs versus GMIL4 Mo-DCs was compared at the end of the differentiation process (6 days), revealing marked differences between them (Figure S8G; Table S4). Mo-DCs obtained in the presence of GM-CSF plus temsirolimus and/or GW9662 displayed a higher expression of different transcription factors such as *SIX5*, *RUNX1*, *ZNF608*, *FOXP4*, and the DNA methyltransferase *DNMT1*. Conversely, GMIL4 Mo-DCs showed a higher expression of several transcription factors including *IRF8*, *AHR*, *MAFB*, and *KLF4*.

GSEA revealed that GMT Mo-DCs and GMGW Mo-DCs, compared with GMIL4 Mo-DCs, showed an increased expression of genes associated with innate immune sensing pathways, especially *NOD*, *RIG1*, and *STING1* (cytosolic DNA sensing) (Figure 4E; Table S4). By exploring the genes responsible for this enrichment, we found that GW9662 and temsirolimus promoted the differentiation of Mo-DCs with an increased expression of type I IFN signature genes (*IFIT1*, *IFIT3*, *IFITM1*, *IFITM2*, *ISG15*,

Figure 4. Mo-DCs differentiated in the presence of GM-CSF and IL-4 or GM-CSF and inhibitors of mTORC1 and/or PPARγ show a very different transcriptional signature

(A) Normalized expression of selected genes comparing monocytes cultured for 8 h in the presence of GM-CSF (50 ng/mL), GM-CSF (50 ng/mL) + IL-4 (30 ng/mL), GM-CSF (50 ng/mL) + temsirolimus (50 nM), GM-CSF (50 ng/mL) + GW9662 (10 μM), or GM-CSF (50 ng/mL) + temsirolimus (50 nM) + GW9662 (10 μM) (n = 4) with sorted CD1a$^+$ CD16$^-$ Mo-DCs obtained after 6 days of culture with GM-CSF + IL-4, GM-CSF + temsirolimus, GM-CSF + GW9662, or GM-CSF + temsirolimus + GW9662 (n = 3).

(B) Heatmap and hierarchical clustering of the top 200 highly variable genes from sorted CD1a$^+$ CD16$^-$ Mo-DCs obtained under different experimental conditions.

(C) Principal-component analysis of *in vitro*-generated M-DCs, peripheral blood cDC1, and cDC2 (GSE108174); CD14$^+$ monocytes, pDCs, and Axl$^+$ DCs (GSE151073).

(D) Volcano plots of comparisons versus GMIL4 Mo-DCs. DEGs were considered if adjusted p value <0.1 and FC > 1.5.

(E) GSEA was performed comparing Mo-DCs generated under different experimental conditions versus GMIL4 Mo-DCs. Significant enrichments ($p < 0.05$) in at least one comparison are shown. The size of the dots represents the NES and the color scale indicates p values.

(F–I) DEGs versus GMIL4 Mo-DCs for type I interferon signature genes or pattern recognition receptor (PRRs) and nuclear factor κB (NF-κB)-associated genes (F), C-type lectin receptors (G), chemokines and cytokines (H), and genes involved in antigen processing and presentation, including CD274 (PD-L1) (I).

(J) Mo-DCs were generated as described in (A). Cells were then washed and cultured for 18 h in the presence or absence of LPS (10 ng/mL). Then, the expression of PD-L1 (CD274) was analyzed by FACS. A representative experiment (left) and bar plots of four experiments (right) are shown (n = 4).

(K) Heatmap displaying the normalized expression of specific genes known to be associated with either immunogenic or tolerogenic DC functional profiles. *$p < 0.05$, **$p < 0.01$, and ***$p < 0.001$.

STING1, and *IFI44L*) as well as *NLRP3*, *MYD88*, *NOD2*, *IL1B*, *IL18*, and *NFKB1*, suggesting an increased activity of inflammasome-dependent pathways (Figure 4F). Since DC function highly depends on their migratory capacity and the use of a wide myriad of phagocytic receptors involved in antigen internalization, we also analyzed the expression of genes involved in these processes. Compared with GMIL4 Mo-DCs, both GMT Mo-DCs and GMGW Mo-DCs displayed an enhanced expression of *CLDN1*, *MMP2*, *ICAM1*, *ITGA4* (CD49d), and *RHOH*, molecules that have been associated with cell-to-cell and cell-to-matrix interactions.[55,56] Interestingly, ITGA4 has been associated with the acquisition of a more mature phenotype in Mo-DCs.[57] Analysis of endocytic receptors also revealed that GMT Mo-DCs and GMGW Mo-DCs showed an enhanced expression of many C-type lectin receptors, including *CD207*, *CLEC4E*, *CLEC4F*, *CLEC5A*, and the scavenger receptor *CD36*. Conversely, these Mo-DCs showed a decreased expression of macrophage-associated surface molecules such as *CD209* (DC-SIGN), *MARCO*, and MERTK (Figure 4G). In addition, GMT Mo-DCs showed an increased expression of genes associated with ribosome structure and function, compared with GMIL4 Mo-DC (Figure S9A).

Among differentially expressed cytokines, a reduced expression of *IL10* was observed, which was most evident in GMTGW Mo-DCs, together with an enhanced expression of *IL24*, *IL7*, *IL15*, *TNF*, and *TNFSF10* (TRAIL) genes (Figure 4H). Regarding the expression of chemokine and cytokine receptors, we found an increased expression of the α and β chains of the receptor for GM-CSF (*CSF2RA* and *CSF2RB*) and the receptor for CCL20 (*CCR6*), a chemokine involved in the recruitment of DCs in peripheral tissues (Figure S9B). Finally, by exploring the expression of genes associated with antigen processing and presentation, we found that GMT Mo-DCs and GMGW Mo-DCs showed an increased expression of *HLA-DMB*, *HLA-DQB1*, *HLA-DQA1*, and *HLA-DOA* (class II HLA genes), *TAP1* and *TAP2* (involved in antigen presentation to $CD8^+$ T cells), *CD40* and *CD80*, together with a reduced expression of *CD86* (Figure 4I). Interestingly, GMTGW Mo-DCs showed a strikingly low expression of the inhibitory gene *CD274* (programmed death-ligand 1 [PD-L1]). Studies performed by flow cytometry confirmed this finding not only in resting Mo-DCs but also in LPS-treated cells (Figures 4J and S9C).

To evaluate whether changes observed in the expression of PD-L1 were part of a broader transcriptional scenario determining Mo-DC immunogenicity, the expression of genes associated with DC immunogenic or tolerogenic profiles was assessed.[58–69] Among genes associated with a stronger immunogenic profile, we did not find a clear bias, except for the expression *STING*, *IL7*, *IL15*, *CD80*, *CD86*, and *CD40*. By contrast, GMIL4 Mo-DCs displayed an overall higher expression of a number of genes associated with a tolerogenic profile, compared with Mo-DCs generated in the presence of mTORC1 and/or PPARγ inhibitors (Figure 4K). These genes included the T-cell immunoglobulin and ITIM domains (TIGIT) ligands *PVR* (CD115) and *CLEC4G* (LSECtin)[59]; the immunoregulatory lectins *LGALS1* (Galectin-1) and *LGALS3* (Galectin-3)[63]; *ADIPOQ* (adiponectin)[65]; the inhibitory receptor *HAVCR2* (TIM3)[60]; the LAG3 ligand *FGL1* (fibrinogen-like protein 1)[67]; the two ligands known to interact with the inhibitory receptor PD-1, *CD274* (PD-L1) and *PDCD1LG2* (PD-L2)[60,70]; *ALDH1A2* (retinaldehyde dehydrogenase 2)[47,66]; and *VDR* (vitamin D receptor).[58] Finally, we analyzed whether the gene expression signature of GMTGW Mo-DCs predicted a higher survival in human tumors using publicly available data from The Cancer Genome Atlas (TCGA) database. For this analysis, a signature composed of the top 150 upregulated genes comparing GMTGW Mo-DCs versus GMIL4 Mo-DCs (included in Table S4) was used. This signature was shown to be associated with better overall survival in cutaneous melanoma and head and neck carcinomas, but not in other tumors (Figure S10).

DISCUSSION

The identity of the factors that guide the differentiation of monocytes into Mo-Macs or Mo-DCs remains poorly defined. Whether key metabolic pathways such as glycolysis, the TCA cycle, amino acid, lipid metabolism, and mTORC1-dependent pathways might play a decisive role in determining the fate of monocytes remains to be determined. We here report that the pharmacological blockade of the nuclear receptor PPARγ in human monocytes turns GM-CSF into a potent inducer of Mo-DC differentiation. Moreover, the simultaneous blockade of both PPARγ and mTORC1 enabled GM-CSF to induce the differentiation of Mo-DCs with a stronger immunogenic profile and higher phenotypic stability compared with canonical Mo-DCs differentiated by GM-CSF and IL-4.[31] Simultaneous blockade of PPARγ and mTORC1 led to the differentiation of Mo-DCs with a high ability to produce IL-12 without any detectable production of IL-10, to promote the differentiation of Th1 cells, and to induce the expansion of $CD8^+$ T cells in an antigen-dependent manner. Moreover, disruption of these metabolic pathways induced the differentiation of Mo-Macs into Mo-DCs.

The promotion of Mo-DC differentiation induced by PPARγ inhibition occurs in a particular context; i.e., in the presence of GM-CSF. No promotion was observed in monocytes treated with M-CSF or when monocytes were cultured with cytokine cocktails able to induce the differentiation of Mo-DCs, such as GM-CSF/IL4 or M-CSF/IL4/TNF-α. It is well established that PPARγ activation inhibits the production of inflammatory cytokines by monocytes and macrophages.[71] Regarding DCs, most of the previous studies were performed by studying the effect of synthetic PPARγ agonists on Mo-DCs differentiated by GM-CSF and IL-4. Freshly isolated monocytes barely express PPARγ, but its expression is markedly upregulated within a few hours after stimulation by GM-CSF or IL-4.[23] Studies performed by the Nagy L group[33,41,47] have shown that PPARγ activation results in a decreased ability of Mo-DCs to induce antigen-specific T cell responses impairing both the production of IL-12 and their ability to induce the differentiation of $CD4^+$ T cells into a Th1 profile. Consistent with these observations, other laboratories reported that PPARγ activation inhibits the activation of Mo-DCs through TLRs or CD40L.[72–74] Our results show that the PPARγ inhibitor GW9662 does not affect Mo-DC differentiation induced by GM-CSF and IL-4. However, this process was significantly inhibited by the synthetic PPARγ agonist rosiglitazone, suggesting that PPARγ-dependent pathways are able to suppress Mo-DC differentiation induced by GM-CSF and IL-4 when these

pathways are strongly activated by exogenous stimuli. Together, these observations suggest PPARγ inhibition promotes the acquisition of an inflammatory signature by DCs. However, it should be noted that PPARγ inhibition might compromise some DC functions that require the functionality of this pathway. Among them are mannose receptor-mediated endocytosis, the uptake of apoptotic cells mediated by the scavenger receptor CD36, and the activation and expansion of invariant natural killer T (iNKT) cells induced by CD1d molecules.[23,75–78]

Transcriptomic analysis performed at either early time points, as well as at the end of the differentiation process, showed critical differences in the gene expression profile between GM-CSF-treated monocytes cultured either in the presence of IL-4 or in the presence of PPARγ and/or mTORC1 inhibitors. GSEA performed at 8 h of culture showed that the TCA cycle, steroid biosynthesis, and PPAR signaling-associated genes were upregulated by IL-4 and downregulated by either temsirolimus or GW9662, suggesting a clear contrast in early metabolic pathways activated in the course of Mo-DC differentiation. A sharp contrast was also observed when analyzing the expression of transcription factors, including those involved in DC differentiation. In fact, we observed that the differentiation of GMIL4 Mo-DCs was associated with an early enrichment in the expression of BATF3, NFIL3, and IRF8 compared with Mo-DCs differentiated in the presence of temsirolimus and/or GW9662. Interestingly, these three transcription factors have been associated with the differentiation of cDC1 cells.[52,79–81] By contrast, differentiation of Mo-DCs performed in the presence of temsirolimus and/or GW9662 was associated with an increased expression of IRF4, a transcription factor required for both the differentiation of Mo-DCs and cDC2s.[10,34,52,82–84] These observations suggest that activation of divergent differentiation pathways occurs early in the differentiation process. Interestingly, we also found that the combined blockade of PPARγ and mTORC1 displayed additive effects on the expression of a set of genes that belong to the nuclear receptor superfamily,[85,86] including the retinoid X receptor alpha *RXRA* and members of the NR4A subfamily such as *NR4A1*, *NR4A2*, and *NR4A3*.[53,87] NR4A subfamily members are orphan receptors classically described as early and intermediate response genes that are upregulated by different kinds of stimuli, including growth factors, cytokines, and fatty acids.[53,88,89] Interestingly, it has been shown that NR4A receptors play important roles in myeloid cell differentiation.[53] Studies performed in mice suggest that NR4A1 is necessary for the transition of $Ly6C_{high}$ into $Ly6C_{low}$ monocytes,[82,90] while NR4A3 is involved in the generation of Mo-DCs.[91] Furthermore, the involvement of NR4A receptors in the regulation of cell metabolism[87,92,93] suggests that they might be involved in the promoting effect induced by mTORC1 and/or PPARγ blockade on Mo-DC differentiation.

Transcriptomic studies of FACS-sorted Mo-DCs performed at the end of the differentiation process (6 days) also showed major differences. Compared with GMIL4 Mo-DCs, either GMT, GMGW, or GMTGW Mo-DCs showed an increased expression of type I IFN and inflammasome-associated genes together with an enhanced expression of many genes coding for C-type lectin receptors. Interestingly, we found that GMIL4 Mo-DCs were enriched in the expression of genes associated with a macrophage-like profile and a tolerogenic signature, compared with GMT, GMGW, and GMTGW Mo-DCs. Genes associated with a macrophage-like profile included *CD163*, *MARCO*, *MAFB*, *CR1*, *MERTK*, *FCGR3A*, and *CSF1R*. Among others, genes associated with a tolerogenic profile included *ALDH1A2*, *VDR*, *ADIPOQ* (adiponectin), *IL10*, *WNT5A*, *CD274* (PD-L1), *HAVCR2* (TIM3), *LGALS1* (Galectin-1), *LGALS3* (Galectin-3), and *SOCS1* (suppressor of cytokine signaling 1). Another particular feature of Mo-DCs differentiated in the presence of temsirolimus and/or GW9662, is the expression of Langerin (CD207) in a subpopulation of the cells. While under steady state, lineage tracing studies performed in mice showed that Langerhans cells arise from primitive macrophages of the yolk sac and fetal liver, and it is well established that, during inflammation, monocytes recruited to the inflamed skin can differentiate into $Langerin^+$ cells through a pathway dependent on the expression of transcription factors *RUNX3* and *SPI1* (PU.1),[94–96] two genes that we found upregulated in Mo-DCs differentiated in the presence of temsirolimus and/or GW9662. Interestingly, Langerin expression in mice and human DCs has been not only associated with bona fide Langerhans cells but also with other cells among the DC spectrum.[97] While $Langerin^+$ DCs can be found in a subset of $CD8a^+/CD103^+$ $XCR1^+$ cDC1 cells in mouse lymphoid and peripheral tissues,[97,98] human $Langerin^+$ DCs are not associated with the characteristic transcriptional signature of cDC1 cells but with cDC2 DCs.[99]

Mo-DCs differentiated in the presence of both temsirolimus and GW9662 showed a set of particular properties compared not only with GMIL4 Mo-DCs but also with GMT and GMGW Mo-DCs. This population of Mo-DCs showed the highest capacity to produce IL-12 (in the absence of IL-10 production) and to induce the production of Th1 cytokines together with a remarkable phenotypic stability. Moreover, we found that simultaneous inhibition of mTORC1 and PPARγ, but not IL-4 or individual inhibition of mTORC1 or PPARγ, enabled GM-CSF to efficiently induce the differentiation of Mo-Macs into Mo-DCs. It would be very relevant to study whether a similar phenomenon could be observed *in vivo*, particularly in the scenario of cancer immunity.

DC-based vaccines are promising immunotherapeutic strategies that have been mainly tested in the context of cancer immunotherapy.[68,100] Despite their good safety profile and ability to elicit detectable antigen-specific responses in patients, clinical outcomes have been rather disappointing.[101] Different hypotheses might explain the limited clinical benefit of current DC vaccine regimes, among them the acquisition of a tolerogenic profile by transferred DCs in response to environmental factors found in the tumor environment, such as PGE2, IL-10, TGF-β, M-CSF, and Galectin-1.[63,102,103] Our present results suggest that Mo-DCs differentiated *in vitro* with GM-CSF in the presence of mTORC1 and PPARγ inhibitors might display a stronger anti-tumor response compared with Mo-DCs obtained by conventional methods, based on the use of GM-CSF and IL-4.

Limitations of the study

Our study has a number of limitations. Pharmacological modulation was used as a strategy to target mTORC1 and PPARγ

pathways, instead of gene knockout approaches. Moreover, we did not perform gene knockdown experiments to determine whether the gene expression changes observed along the process of Mo-DC differentiation actually reflect a role of some of these genes in the differentiation process or in the acquisition of an inflammatory or tolerogenic signatures. Moreover, we did not perform *in vivo* experiments to determine the therapeutic properties of Mo-DCs differentiated in the presence of mTORC1 and PPARγ inhibitors.

STAR★METHODS

Detailed methods are provided in the online version of this paper and include the following:

- KEY RESOURCES TABLE
- RESOURCE AVAILABILITY
  - Lead contact
  - Data and code availability
- EXPERIMENTAL MODEL AND SUBJECT DETAILS
  - Human blood samples
- METHOD DETAILS
  - Cell isolation
  - Cell culture
  - Flow cytometry and cell sorting
  - Fatty acid uptake assay
  - Phagocytosis assay
  - OVA-DQ processing assay
  - Reanalysis of microarray and scRNAseq datasets
  - Quantitative Real-Time PCR (qPCR)
  - Cell lysates and immunoblots
  - RNAseq library preparation
  - RNAseq data analysis
  - Fluorescence and confocal microscopy
  - Measurement of cytokines by ELISA
  - Mixed lymphocyte reaction proliferation assays
  - Antigen-specific CD8 T cell activation assay
  - Chemicals
- QUANTIFICATION AND STATISTICAL ANALYSIS

SUPPLEMENTAL INFORMATION

Supplemental information can be found online at https://doi.org/10.1016/j.celrep.2023.112156.

ACKNOWLEDGMENTS

We gratefully acknowledge the contribution of Virginia González Polo PhD for her assistance in cell sorting experiments, as well as the Genome Technologies Service at The Jackson Laboratory for expert assistance with the work described herein.

This work was supported by grants from the Agencia Nacional de Promoción Científica y Tecnológica, Argentina (PICT 2017-1616 and PICT 2018–02844), and Universidad de Buenos Aires (UBA), Argentina (UBACyT 20020170100573BA) to J.G.

AUTHOR CONTRIBUTIONS

F.E.D., D.U., and J.G. conceptualized the work. F.E.D. performed most of the experiments and data analysis. F.E.D, G.R., D.U., and J.G. wrote the manuscript. I.M., L.B., and T.D.M. performed ELISA assays, cell isolation, flow cytometry acquisition, and microscopic analysis. A.T., R.M., and D.U. contributed to the design of the experiments and the analysis of transcriptomic data. F.E.D., R.M., D.U., and J.G. supervised the project. D.U. and J.G. acquired the funding.

DECLARATION OF INTERESTS

The authors declare no competing interests.

INCLUSION AND DIVERSITY

We support inclusive, diverse, and equitable conduct of research.

Received: September 19, 2022
Revised: December 29, 2022
Accepted: February 8, 2023
Published: February 26, 2023

REFERENCES

1. Banchereau, J., and Steinman, R.M. (1998). Dendritic cells and the control of immunity. Nature *392*, 245–252. https://doi.org/10.1038/32588.
2. Guilliams, M., Ginhoux, F., Jakubzick, C., Naik, S.H., Onai, N., Schraml, B.U., Segura, E., Tussiwand, R., and Yona, S. (2014). Dendritic cells, monocytes and macrophages: a unified nomenclature based on ontogeny. Nat. Rev. Immunol. *14*, 571–578. https://doi.org/10.1038/nri3712.
3. Cabeza-Cabrerizo, M., Cardoso, A., Minutti, C.M., Pereira da Costa, M., and Reis E Sousa, C. (2021). Dendritic cells revisited. Annu. Rev. Immunol. *39*, 131–166. https://doi.org/10.1146/annurev-immunol-061020-053707.
4. Steinman, R.M. (2012). Decisions about dendritic cells: past, present, and future. Annu. Rev. Immunol. *30*, 1–22. https://doi.org/10.1146/annurev-immunol-100311-102839.
5. Merad, M., Sathe, P., Helft, J., Miller, J., and Mortha, A. (2013). The dendritic cell lineage: ontogeny and function of dendritic cells and their subsets in the steady state and the inflamed setting. Annu. Rev. Immunol. *31*, 563–604. https://doi.org/10.1146/annurev-immunol-020711-074950.
6. Liu, K., Victora, G.D., Schwickert, T.A., Guermonprez, P., Meredith, M.M., Yao, K., Chu, F.-F., Randolph, G.J., Rudensky, A.Y., and Nussenzweig, M. (2009). In vivo analysis of dendritic cell development and homeostasis. Science *324*, 392–397. https://doi.org/10.1126/science.1170540.
7. Boltjes, A., and van Wijk, F. (2014). Human dendritic cell functional specialization in steady-state and inflammation. Front. Immunol. *5*, 131. https://doi.org/10.3389/fimmu.2014.00131.
8. Gerhard, G.M., Bill, R., Messemaker, M., Klein, A.M., and Pittet, M.J. (2021). Tumor-infiltrating dendritic cell states are conserved across solid human cancers. J. Exp. Med. *218*, e20200264. https://doi.org/10.1084/jem.20200264.
9. Randolph, G.J., Inaba, K., Robbiani, D.F., Steinman, R.M., and Muller, W.A. (1999). Differentiation of phagocytic monocytes into lymph node dendritic cells in vivo. Immunity *11*, 753–761. https://doi.org/10.1016/S1074-7613(00)80149-1.
10. Segura, E., and Amigorena, S. (2013). Inflammatory dendritic cells in mice and humans. Trends Immunol. *34*, 440–445. https://doi.org/10.1016/j.it.2013.06.001.
11. Shortman, K., and Naik, S.H. (2007). Steady-state and inflammatory dendritic-cell development. Nat. Rev. Immunol. *7*, 19–30. https://doi.org/10.1038/nri1996.
12. Buck, M.D., Sowell, R.T., Kaech, S.M., and Pearce, E.L. (2017). Metabolic instruction of immunity. Cell *169*, 570–586. https://doi.org/10.1016/j.cell.2017.04.004.

13. Laplante, M., and Sabatini, D.M. (2012). mTOR signaling in growth control and disease. Cell *149*, 274–293. https://doi.org/10.1016/j.cell.2012.03.017.

14. Erra Díaz, F., Ochoa, V., Merlotti, A., Dantas, E., Mazzitelli, I., Gonzalez Polo, V., Sabatté, J., Amigorena, S., Segura, E., and Geffner, J. (2020). Extracellular acidosis and mTOR inhibition drive the differentiation of human monocyte-derived dendritic cells. Cell Rep. *31*, 107613. https://doi.org/10.1016/j.celrep.2020.107613.

15. Coillard, A., Guyonnet, L., De Juan, A., Cros, A., and Segura, E. (2021). TLR or NOD receptor signaling skews monocyte fate decision via distinct mechanisms driven by mTOR and miR-155. Proc. Natl. Acad. Sci. USA *118*, e2109225118. https://doi.org/10.1073/pnas.2109225118.

16. Hernandez-Quiles, M., Broekema, M.F., and Kalkhoven, E. (2021). PPARgamma in metabolism, immunity, and cancer: unified and diverse mechanisms of action. Front. Endocrinol. *12*, 624112. https://doi.org/10.3389/fendo.2021.624112.

17. Lefterova, M.I., Haakonsson, A.K., Lazar, M.A., and Mandrup, S. (2014). PPARγ and the global map of adipogenesis and beyond. Trends Endocrinol. Metabol. *25*, 293–302. https://doi.org/10.1016/j.tem.2014.04.001.

18. Lehrke, M., and Lazar, M.A. (2005). The many faces of PPARgamma. Cell *123*, 993–999. https://doi.org/10.1016/j.cell.2005.11.026.

19. Bouhlel, M.A., Derudas, B., Rigamonti, E., Dièvart, R., Brozek, J., Haulon, S., Zawadzki, C., Jude, B., Torpier, G., Marx, N., et al. (2007). PPARγ activation primes human monocytes into alternative M2 macrophages with anti-inflammatory properties. Cell Metabol. *6*, 137–143. https://doi.org/10.1016/j.cmet.2007.06.010.

20. Cipolletta, D., Feuerer, M., Li, A., Kamei, N., Lee, J., Shoelson, S.E., Benoist, C., and Mathis, D. (2012). PPAR-γ is a major driver of the accumulation and phenotype of adipose tissue Treg cells. Nature *486*, 549–553. https://doi.org/10.1038/nature11132.

21. Klotz, L., Burgdorf, S., Dani, I., Saijo, K., Flossdorf, J., Hucke, S., Alferink, J., Nowak, N., Beyer, M., Mayer, G., et al. (2009). The nuclear receptor PPARγ selectively inhibits Th17 differentiation in a T cell–intrinsic fashion and suppresses CNS autoimmunity. J. Exp. Med. *206*, 2079–2089. https://doi.org/10.1084/jem.20082771.

22. Natarajan, C., and Bright, J.J. (2002). Peroxisome proliferator-activated receptor-gamma agonists inhibit experimental allergic encephalomyelitis by blocking IL-12 production, IL-12 signaling and Th1 differentiation. Gene Immun. *3*, 59–70. https://doi.org/10.1038/sj.gene.6363832.

23. Szatmari, I., Gogolak, P., Im, J.S., Dezso, B., Rajnavolgyi, E., and Nagy, L. (2004). Activation of PPARgamma specifies a dendritic cell subtype capable of enhanced induction of iNKT cell expansion. Immunity *21*, 95–106. https://doi.org/10.1016/j.immuni.2004.06.003.

24. Franklin, R.A., and Li, M.O. (2016). Ontogeny of tumor-associated macrophages and its implication in cancer regulation. Trends Cancer *2*, 20–34. https://doi.org/10.1016/j.trecan.2015.11.004.

25. Franklin, R.A., Liao, W., Sarkar, A., Kim, M.V., Bivona, M.R., Liu, K., Pamer, E.G., and Li, M.O. (2014). The cellular and molecular origin of tumor-associated macrophages. Science *344*, 921–925. https://doi.org/10.1126/science.1252510.

26. Ma, Y., Adjemian, S., Mattarollo, S.R., Yamazaki, T., Aymeric, L., Yang, H., Portela Catani, J.P., Hannani, D., Duret, H., Steegh, K., et al. (2013). Anticancer chemotherapy-induced intratumoral recruitment and differentiation of antigen-presenting cells. Immunity *38*, 729–741. https://doi.org/10.1016/j.immuni.2013.03.003.

27. Segura, E., Touzot, M., Bohineust, A., Cappuccio, A., Chiocchia, G., Hosmalin, A., Dalod, M., Soumelis, V., and Amigorena, S. (2013). Human inflammatory dendritic cells induce Th17 cell differentiation. Immunity *38*, 336–348. https://doi.org/10.1016/j.immuni.2012.10.018.

28. Daynes, R.A., and Jones, D.C. (2002). Emerging roles of PPARS in inflammation and immunity. Nat. Rev. Immunol. *2*, 748–759. https://doi.org/10.1038/nri912.

29. Cheng, S., Li, Z., Gao, R., Xing, B., Gao, Y., Yang, Y., Qin, S., Zhang, L., Ouyang, H., Du, P., et al. (2021). A pan-cancer single-cell transcriptional atlas of tumor infiltrating myeloid cells. Cell *184*, 792–809.e23. https://doi.org/10.1016/j.cell.2021.01.010.

30. Sander, J., Schmidt, S.V., Cirovic, B., McGovern, N., Papantonopoulou, O., Hardt, A.-L., Aschenbrenner, A.C., Kreer, C., Quast, T., Xu, A.M., et al. (2017). Cellular differentiation of human monocytes is regulated by time-dependent interleukin-4 signaling and the transcriptional regulator NCOR2. Immunity *47*, 1051–1066.e12. https://doi.org/10.1016/j.immuni.2017.11.024.

31. Sallusto, F., and Lanzavecchia, A. (1994). Efficient presentation of soluble antigen by cultured human dendritic cells is maintained by granulocyte/macrophage colony-stimulating factor plus interleukin 4 and downregulated by tumor necrosis factor alpha. J. Exp. Med. *179*, 1109–1118. https://doi.org/10.1084/jem.179.4.1109.

32. Ray, R., and Rai, V. (2017). Lysophosphatidic acid converts monocytes into macrophages in both mice and humans. Blood *129*, 1177–1183. https://doi.org/10.1182/blood-2016-10-743757.

33. Szatmari, I., Töröcsik, D., Agostini, M., Nagy, T., Gurnell, M., Barta, E., Chatterjee, K., and Nagy, L. (2007). PPARgamma regulates the function of human dendritic cells primarily by altering lipid metabolism. Blood *110*, 3271–3280. https://doi.org/10.1182/blood-2007-06-096222.

34. Goudot, C., Coillard, A., Villani, A.-C., Gueguen, P., Cros, A., Sarkizova, S., Tang-Huau, T.-L., Bohec, M., Baulande, S., Hacohen, N., et al. (2017). Aryl hydrocarbon receptor controls monocyte differentiation into dendritic cells versus macrophages. Immunity *47*, 582–596.e6. https://doi.org/10.1016/j.immuni.2017.08.016.

35. Martinez, F.O., Gordon, S., Locati, M., and Mantovani, A. (2006). Transcriptional profiling of the human monocyte-to-macrophage differentiation and polarization: new molecules and patterns of gene expression. J. Immunol. *177*, 7303–7311. https://doi.org/10.4049/jimmunol.177.10.7303.

36. Rodriguez, R.M., Suarez-Alvarez, B., Lavín, J.L., Ascensión, A.M., Gonzalez, M., Lozano, J.J., Raneros, A.B., Bulnes, P.D., Vidal-Castiñeira, J.R., Huidobro, C., et al. (2019). Signal integration and transcriptional regulation of the inflammatory response mediated by the GM-/M-CSF signaling Axis in human monocytes. Cell Rep. *29*, 860–872.e5. https://doi.org/10.1016/j.celrep.2019.09.035.

37. Palucka, K.A., Taquet, N., Sanchez-Chapuis, F., and Gluckman, J.C. (1998). Dendritic cells as the terminal stage of monocyte differentiation. J. Immunol. *160*, 4587–4595.

38. Leesnitzer, L.M., Parks, D.J., Bledsoe, R.K., Cobb, J.E., Collins, J.L., Consler, T.G., Davis, R.G., Hull-Ryde, E.A., Lenhard, J.M., Patel, L., et al. (2002). Functional consequences of cysteine modification in the ligand binding sites of peroxisome proliferator activated receptors by GW9662. Biochemistry *41*, 6640–6650. https://doi.org/10.1021/bi0159581.

39. Kalinski, P. (2012). Regulation of immune responses by prostaglandin E_2. J. Immunol. *188*, 21–28. https://doi.org/10.4049/jimmunol.1101029.

40. Nassar, G.M., Morrow, J.D., Roberts, L.J., Lakkis, F.G., and Badr, K.F. (1994). Induction of 15-lipoxygenase by interleukin-13 in human blood monocytes. J. Biol. Chem. *269*, 27631–27634.

41. Szanto, A., Balint, B.L., Nagy, Z.S., Barta, E., Dezso, B., Pap, A., Szeles, L., Poliska, S., Oros, M., Evans, R.M., et al. (2010). STAT6 transcription factor is a facilitator of the nuclear receptor PPARγ-regulated gene expression in macrophages and dendritic cells. Immunity *33*, 699–712. https://doi.org/10.1016/j.immuni.2010.11.009.

42. Huyton, T., Göttmann, W., Bade-Döding, C., Paine, A., and Blasczyk, R. (2011). The T/NK cell co-stimulatory molecule SECTM1 is an IFN "early response gene" that is negatively regulated by LPS in Human monocytic cells. Biochim. Biophys. Acta *1810*, 1294–1301. https://doi.org/10.1016/j.bbagen.2011.06.020.

43. Wang, P., Lv, C., Zhang, T., Liu, J., Yang, J., Guan, F., and Hong, T. (2017). FOXQ1 regulates senescence-associated inflammation via

activation of SIRT1 expression. Cell Death Dis. *8*, e2946. https://doi.org/10.1038/cddis.2017.340.

44. Furuhashi, M., Saitoh, S., Shimamoto, K., and Miura, T. (2014). Fatty acid-binding protein 4 (FABP4): pathophysiological insights and potent clinical biomarker of metabolic and cardiovascular diseases. Clin. Med. Insights Cardiol. *8*, 23–33. https://doi.org/10.4137/CMC.S17067.
45. Persaud, L., De Jesus, D., Brannigan, O., Richiez-Paredes, M., Huaman, J., Alvarado, G., Riker, L., Mendez, G., Dejoie, J., and Sauane, M. (2016). Mechanism of action and applications of interleukin 24 in immunotherapy. Int. J. Mol. Sci. *17*, 869. https://doi.org/10.3390/ijms17060869.
46. Guo, B., Huang, X., Lee, M.R., Lee, S.A., and Broxmeyer, H.E. (2018). Antagonism of PPAR-γ signaling expands human hematopoietic stem and progenitor cells by enhancing glycolysis. Nat. Med. *24*, 360–367. https://doi.org/10.1038/nm.4477.
47. Szatmari, I., Pap, A., Rühl, R., Ma, J.-X., Illarionov, P.A., Besra, G.S., Rajnavolgyi, E., Dezso, B., and Nagy, L. (2006). PPARgamma controls CD1d expression by turning on retinoic acid synthesis in developing human dendritic cells. J. Exp. Med. *203*, 2351–2362. https://doi.org/10.1084/jem.20060141.
48. Zhou, Z., Li, W., Song, Y., Wang, L., Zhang, K., Yang, J., Zhang, W., Su, H., and Zhang, Y. (2013). Growth differentiation factor-15 suppresses maturation and function of dendritic cells and inhibits tumor-specific immune response. PLoS One *8*, e78618. https://doi.org/10.1371/journal.pone.0078618.
49. Bergenfelz, C., Janols, H., Wullt, M., Jirström, K., Bredberg, A., and Leandersson, K. (2013). Wnt5a inhibits human monocyte-derived myeloid dendritic cell generation. Scand. J. Immunol. *78*, 194–204. https://doi.org/10.1111/sji.12075.
50. Valencia, J., Hernández-López, C., Martínez, V.G., Hidalgo, L., Zapata, A.G., Vicente, Á., Varas, A., and Sacedón, R. (2011). Wnt5a skews dendritic cell differentiation to an unconventional phenotype with tolerogenic features. J. Immunol. *187*, 4129–4139. https://doi.org/10.4049/jimmunol.1101243.
51. Angela, M., Endo, Y., Asou, H.K., Yamamoto, T., Tumes, D.J., Tokuyama, H., Yokote, K., and Nakayama, T. (2016). Fatty acid metabolic reprogramming via mTOR-mediated inductions of PPARγ directs early activation of T cells. Nat. Commun. *7*, 13683. https://doi.org/10.1038/ncomms13683.
52. Murphy, T.L., Grajales-Reyes, G.E., Wu, X., Tussiwand, R., Briseño, C.G., Iwata, A., Kretzer, N.M., Durai, V., and Murphy, K.M. (2016). Transcriptional control of dendritic cell development. Annu. Rev. Immunol. *34*, 93–119. https://doi.org/10.1146/annurev-immunol-032713-120204.
53. Boulet, S., Le Corre, L., Odagiu, L., and Labrecque, N. (2022). Role of NR4A family members in myeloid cells and leukemia. Curr. Res. Immunol. *3*, 23–36. https://doi.org/10.1016/j.crimmu.2022.02.001.
54. Perlmann, T., and Jansson, L. (1995). A novel pathway for vitamin A signaling mediated by RXR heterodimerization with NGFI-B and NURR1. Genes Dev. *9*, 769–782. https://doi.org/10.1101/gad.9.7.769.
55. Scholer, A., Hugues, S., Boissonnas, A., Fetler, L., and Amigorena, S. (2008). Intercellular adhesion molecule-1-dependent stable interactions between T cells and dendritic cells determine CD8+ T cell memory. Immunity *28*, 258–270. https://doi.org/10.1016/j.immuni.2007.12.016.
56. Zimmerli, S.C., and Hauser, C. (2007). Langerhans cells and lymph node dendritic cells express the tight junction component claudin-1. J. Invest. Dermatol. *127*, 2381–2390. https://doi.org/10.1038/sj.jid.5700882.
57. Puig-Kröger, A., Sanz-Rodríguez, F., Longo, N., Sánchez-Mateos, P., Botella, L., Teixidó, J., Bernabéu, C., and Corbí, A.L. (2000). Maturation-dependent expression and function of the CD49d integrin on monocyte-derived human dendritic cells. J. Immunol. *165*, 4338–4345. https://doi.org/10.4049/jimmunol.165.8.4338.
58. Català-Moll, F., Ferreté-Bonastre, A.G., Godoy-Tena, G., Morante-Palacios, O., Ciudad, L., Barberà, L., Fondelli, F., Martínez-Cáceres, E.M., Rodríguez-Ubreva, J., Li, T., and Ballestar, E. (2022). Vitamin D receptor, STAT3, and TET2 cooperate to establish tolerogenesis. Cell Rep. *38*, 110244. https://doi.org/10.1016/j.celrep.2021.110244.
59. Chauvin, J.-M., and Zarour, H.M. (2020). TIGIT in cancer immunotherapy. J. Immunother. Cancer *8*, e000957. https://doi.org/10.1136/jitc-2020-000957.
60. Cogdill, A.P., Andrews, M.C., and Wargo, J.A. (2017). Hallmarks of response to immune checkpoint blockade. Br. J. Cancer *117*, 1–7. https://doi.org/10.1038/bjc.2017.136.
61. Devalaraja, S., To, T.K.J., Folkert, I.W., Natesan, R., Alam, M.Z., Li, M., Tada, Y., Budagyan, K., Dang, M.T., Zhai, L., et al. (2020). Tumor-derived retinoic acid regulates intratumoral monocyte differentiation to promote immune suppression. Cell *180*, 1098–1114.e16. https://doi.org/10.1016/j.cell.2020.02.042.
62. Mattei, F., Schiavoni, G., Belardelli, F., and Tough, D.F. (2001). IL-15 is expressed by dendritic cells in response to type I IFN, double-stranded RNA, or lipopolysaccharide and promotes dendritic cell activation. J. Immunol. *167*, 1179–1187. https://doi.org/10.4049/jimmunol.167.3.1179.
63. Rabinovich, G.A., and Toscano, M.A. (2009). Turning "sweet" on immunity: galectin–glycan interactions in immune tolerance and inflammation. Nat. Rev. Immunol. *9*, 338–352. https://doi.org/10.1038/nri2536.
64. Stary, G., Bangert, C., Tauber, M., Strohal, R., Kopp, T., and Stingl, G. (2007). Tumoricidal activity of TLR7/8-activated inflammatory dendritic cells. J. Exp. Med. *204*, 1441–1451. https://doi.org/10.1084/jem.20070021.
65. Tsang, J.Y.S., Li, D., Ho, D., Peng, J., Xu, A., Lamb, J., Chen, Y., and Tam, P.K.H. (2011). Novel immunomodulatory effects of adiponectin on dendritic cell functions. Int. Immunopharm. *11*, 604–609. https://doi.org/10.1016/j.intimp.2010.11.009.
66. Vander Lugt, B., Riddell, J., Khan, A.A., Hackney, J.A., Lesch, J., DeVoss, J., Weirauch, M.T., Singh, H., and Mellman, I. (2017). Transcriptional determinants of tolerogenic and immunogenic states during dendritic cell maturation. J. Cell Biol. *216*, 779–792. https://doi.org/10.1083/jcb.201512012.
67. Wang, J., Sanmamed, M.F., Datar, I., Su, T.T., Ji, L., Sun, J., Chen, L., Chen, Y., Zhu, G., Yin, W., et al. (2019). Fibrinogen-like protein 1 is a major immune inhibitory ligand of LAG-3. Cell *176*, 334–347.e12. https://doi.org/10.1016/j.cell.2018.11.010.
68. Wculek, S.K., Cueto, F.J., Mujal, A.M., Melero, I., Krummel, M.F., and Sancho, D. (2020). Dendritic cells in cancer immunology and immunotherapy. Nat. Rev. Immunol. *20*, 7–24. https://doi.org/10.1038/s41577-019-0210-z.
69. Woo, S.-R., Fuertes, M.B., Corrales, L., Spranger, S., Furdyna, M.J., Leung, M.Y.K., Duggan, R., Wang, Y., Barber, G.N., Fitzgerald, K.A., et al. (2014). STING-dependent cytosolic DNA sensing mediates innate immune recognition of immunogenic tumors. Immunity *41*, 830–842. https://doi.org/10.1016/j.immuni.2014.10.017.
70. Garris, C.S., Arlauckas, S.P., Kohler, R.H., Trefny, M.P., Garren, S., Piot, C., Engblom, C., Pfirschke, C., Siwicki, M., Gungabeesoon, J., et al. (2018). Successful anti-PD-1 cancer immunotherapy requires T cell-dendritic cell crosstalk involving the cytokines IFN-γ and IL-12. Immunity *49*, 1148–1161.e7. https://doi.org/10.1016/j.immuni.2018.09.024.
71. Alleva, D.G., Johnson, E.B., Lio, F.M., Boehme, S.A., Conlon, P.J., and Crowe, P.D. (2002). Regulation of murine macrophage proinflammatory and anti-inflammatory cytokines by ligands for peroxisome proliferator-activated receptor-gamma: counter-regulatory activity by IFN-gamma. J. Leukoc. Biol. *71*, 677–685.
72. Appel, S., Mirakaj, V., Bringmann, A., Weck, M.M., Grünebach, F., and Brossart, P. (2005). PPAR-gamma agonists inhibit toll-like receptor-mediated activation of dendritic cells via the MAP kinase and NF-kappaB pathways. Blood *106*, 3888–3894. https://doi.org/10.1182/blood-2004-12-4709.

73. Gosset, P., Charbonnier, A.S., Delerive, P., Fontaine, J., Staels, B., Pestel, J., Tonnel, A.B., and Trottein, F. (2001). Peroxisome proliferator-activated receptor gamma activators affect the maturation of human monocyte-derived dendritic cells. Eur. J. Immunol. *31*, 2857–2865. https://doi.org/10.1002/1521-4141(2001010)31:10<2857::aid-immu2857>3.0.co;2-x.

74. Nencioni, A., Grünebach, F., Zobywlaski, A., Denzlinger, C., Brugger, W., and Brossart, P. (2002). Dendritic cell immunogenicity is regulated by peroxisome proliferator-activated receptor gamma. J. Immunol. *169*, 1228–1235. https://doi.org/10.4049/jimmunol.169.3.1228.

75. Gyöngyösi, A., and Nagy, L. (2008). Potential therapeutic use of PPAR γ -programed human monocyte-derived dendritic cells in cancer vaccination therapy. PPAR Res. *2008*, 473804–473810. https://doi.org/10.1155/2008/473804.

76. Nagy, L., Szanto, A., Szatmari, I., and Széles, L. (2012). Nuclear hormone receptors enable macrophages and dendritic cells to sense their lipid environment and shape their immune response. Physiol. Rev. *92*, 739–789. https://doi.org/10.1152/physrev.00004.2011.

77. Cuaranta-Monroy, I., Kiss, M., Simandi, Z., and Nagy, L. (2015). Genome-wide effects of peroxisome proliferator-activated receptor gamma in macrophages and dendritic cells - revealing complexity through systems biology. Eur. J. Clin. Invest. *45*, 964–975. https://doi.org/10.1111/eci.12491.

78. Daniel, B., Nagy, G., Czimmerer, Z., Horvath, A., Hammers, D.W., Cuaranta-Monroy, I., Poliska, S., Tzerpos, P., Kolostyak, Z., Hays, T.T., et al. (2018). The nuclear receptor PPARγ controls progressive macrophage polarization as a ligand-insensitive epigenomic ratchet of transcriptional memory. Immunity *49*, 615–626.e6. https://doi.org/10.1016/j.immuni.2018.09.005.

79. Ginhoux, F., Liu, K., Helft, J., Bogunovic, M., Greter, M., Hashimoto, D., Price, J., Yin, N., Bromberg, J., Lira, S.A., et al. (2009). The origin and development of nonlymphoid tissue CD103+ DCs. J. Exp. Med. *206*, 3115–3130. https://doi.org/10.1084/jem.20091756.

80. Grajales-Reyes, G.E., Iwata, A., Albring, J., Wu, X., Tussiwand, R., Kc, W., Kretzer, N.M., Briseño, C.G., Durai, V., Bagadia, P., et al. (2015). Batf3 maintains autoactivation of Irf8 for commitment of a CD8α+ conventional DC clonogenic progenitor. Nat. Immunol. *16*, 708–717. https://doi.org/10.1038/ni.3197.

81. Liu, T.-T., Kim, S., Desai, P., Kim, D.-H., Huang, X., Ferris, S.T., Wu, R., Ou, F., Egawa, T., Van Dyken, S.J., et al. (2022). Ablation of cDC2 development by triple mutations within the Zeb2 enhancer. Nature *607*, 142–148. https://doi.org/10.1038/s41586-022-04866-z.

82. Briseño, C.G., Haldar, M., Kretzer, N.M., Wu, X., Theisen, D.J., Kc, W., Durai, V., Grajales-Reyes, G.E., Iwata, A., Bagadia, P., et al. (2016). Distinct transcriptional programs control cross-priming in classical and monocyte-derived dendritic cells. Cell Rep. *15*, 2462–2474. https://doi.org/10.1016/j.celrep.2016.05.025.

83. Lewis, K.L., Caton, M.L., Bogunovic, M., Greter, M., Grajkowska, L.T., Ng, D., Klinakis, A., Charo, I.F., Jung, S., Gommerman, J.L., et al. (2011). Notch2 receptor signaling controls functional differentiation of dendritic cells in the spleen and intestine. Immunity *35*, 780–791. https://doi.org/10.1016/j.immuni.2011.08.013.

84. Schlitzer, A., McGovern, N., Teo, P., Zelante, T., Atarashi, K., Low, D., Ho, A.W.S., See, P., Shin, A., Wasan, P.S., et al. (2013). IRF4 transcription factor-dependent CD11b+ dendritic cells in human and mouse control mucosal IL-17 cytokine responses. Immunity *38*, 970–983. https://doi.org/10.1016/j.immuni.2013.04.011.

85. Mangelsdorf, D.J., Thummel, C., Beato, M., Herrlich, P., Schütz, G., Umesono, K., Blumberg, B., Kastner, P., Mark, M., Chambon, P., and Evans, R.M. (1995). The nuclear receptor superfamily: the second decade. Cell *83*, 835–839. https://doi.org/10.1016/0092-8674(95)90199-X.

86. Evans, R.M., and Mangelsdorf, D.J. (2014). Nuclear receptors, RXR, and the big bang. Cell *157*, 255–266. https://doi.org/10.1016/j.cell.2014.03.012.

87. Zhao, Y., and Bruemmer, D. (2010). NR4A orphan nuclear receptors: transcriptional regulators of gene expression in metabolism and vascular biology. Arterioscler. Thromb. Vasc. Biol. *30*, 1535–1541. https://doi.org/10.1161/ATVBAHA.109.191163.

88. Maxwell, M.A., and Muscat, G.E.O. (2006). The NR4A subgroup: immediate early response genes with pleiotropic physiological roles. Nucl. Recept. Signal. *4*, 04002. https://doi.org/10.1621/nrs.04002.

89. Beard, J.A., Tenga, A., and Chen, T. (2015). The interplay of NR4A receptors and the oncogene–tumor suppressor networks in cancer. Cell. Signal. *27*, 257–266. https://doi.org/10.1016/j.cellsig.2014.11.009.

90. Hanna, R.N., Carlin, L.M., Hubbeling, H.G., Nackiewicz, D., Green, A.M., Punt, J.A., Geissmann, F., and Hedrick, C.C. (2011). The transcription factor NR4A1 (Nur77) controls bone marrow differentiation and the survival of Ly6C− monocytes. Nat. Immunol. *12*, 778–785. https://doi.org/10.1038/ni.2063.

91. Boulet, S., Daudelin, J.-F., Odagiu, L., Pelletier, A.-N., Yun, T.J., Lesage, S., Cheong, C., and Labrecque, N. (2019). The orphan nuclear receptor NR4A3 controls the differentiation of monocyte-derived dendritic cells following microbial stimulation. Proc. Natl. Acad. Sci. USA *116*, 15150–15159. https://doi.org/10.1073/pnas.1821296116.

92. Yang, P.B., Hou, P.P., Liu, F.Y., Hong, W.B., Chen, H.Z., Sun, X.Y., Li, P., Zhang, Y., Ju, C.Y., Luo, L.J., et al. (2020). Blocking PPARγ interaction facilitates Nur77 interdiction of fatty acid uptake and suppresses breast cancer progression. Proc. Natl. Acad. Sci. USA *117*, 27412–27422. https://doi.org/10.1073/pnas.2002997117.

93. Koenis, D.S., Medzikovic, L., van Loenen, P.B., van Weeghel, M., Huveneers, S., Vos, M., Evers-van Gogh, I.J., Van den Bossche, J., Speijer, D., Kim, Y., et al. (2018). Nuclear receptor Nur77 limits the macrophage inflammatory response through transcriptional reprogramming of mitochondrial metabolism. Cell Rep. *24*, 2127–2140.e7. https://doi.org/10.1016/j.celrep.2018.07.065.

94. Chopin, M., Seillet, C., Chevrier, S., Wu, L., Wang, H., Morse, H.C., Belz, G.T., and Nutt, S.L. (2013). Langerhans cells are generated by two distinct PU.1-dependent transcriptional networks. J. Exp. Med. *210*, 2967–2980. https://doi.org/10.1084/jem.20130930.

95. Ginhoux, F., and Merad, M. (2010). Ontogeny and homeostasis of Langerhans cells. Immunol. Cell Biol. *88*, 387–392. https://doi.org/10.1038/icb.2010.38.

96. Ginhoux, F., Tacke, F., Angeli, V., Bogunovic, M., Loubeau, M., Dai, X.-M., Stanley, E.R., Randolph, G.J., and Merad, M. (2006). Langerhans cells arise from monocytes in vivo. Nat. Immunol. *7*, 265–273. https://doi.org/10.1038/ni1307.

97. Merad, M., Ginhoux, F., and Collin, M. (2008). Origin, homeostasis and function of Langerhans cells and other langerin-expressing dendritic cells. Nat. Rev. Immunol. *8*, 935–947. https://doi.org/10.1038/nri2455.

98. Idoyaga, J., Suda, N., Suda, K., Park, C.G., and Steinman, R.M. (2009). Antibody to Langerin/CD207 localizes large numbers of CD8alpha+ dendritic cells to the marginal zone of mouse spleen. Proc. Natl. Acad. Sci. USA *106*, 1524–1529. https://doi.org/10.1073/pnas.0812247106.

99. Bigley, V., McGovern, N., Milne, P., Dickinson, R., Pagan, S., Cookson, S., Haniffa, M., and Collin, M. (2015). Langerin-expressing dendritic cells in human tissues are related to CD1c $^{+}$ dendritic cells and distinct from Langerhans cells and CD141 ^{high} XCR1 $^{+}$ dendritic cells. J. Leukoc. Biol. *97*, 627–634. https://doi.org/10.1189/jlb.1HI0714-351R.

100. Mastelic-Gavillet, B., Balint, K., Boudousquie, C., Gannon, P.O., and Kandalaft, L.E. (2019). Personalized dendritic cell vaccines-recent breakthroughs and encouraging clinical results. Front. Immunol. *10*, 766. https://doi.org/10.3389/fimmu.2019.00766.

101. Cintolo, J.A., Datta, J., Mathew, S.J., and Czerniecki, B.J. (2012). Dendritic cell-based vaccines: barriers and opportunities. Future Oncol. *8*, 1273–1299. https://doi.org/10.2217/fon.12.125.

102. Almand, B., Resser, J.R., Lindman, B., Nadaf, S., Clark, J.I., Kwon, E.D., Carbone, D.P., and Gabrilovich, D.I. (2000). Clinical significance of

defective dendritic cell differentiation in cancer. Clin. Cancer Res. *6*, 1755–1766.

103. Gabrilovich, D. (2004). Mechanisms and functional significance of tumour-induced dendritic-cell defects. Nat. Rev. Immunol. *4*, 941–952. https://doi.org/10.1038/nri1498.

104. Love, M.I., Huber, W., and Anders, S. (2014). Moderated estimation of fold change and dispersion for RNA-seq data with DESeq2. Genome Biol. *15*, 550. https://doi.org/10.1186/s13059-014-0550-8.

105. Ritchie, M.E., Phipson, B., Wu, D., Hu, Y., Law, C.W., Shi, W., and Smyth, G.K. (2015). Limma powers differential expression analyses for RNA-sequencing and microarray studies. Nucleic Acids Res. *43*, e47. https://doi.org/10.1093/nar/gkv007.

106. Dobin, A., Davis, C.A., Schlesinger, F., Drenkow, J., Zaleski, C., Jha, S., Batut, P., Chaisson, M., and Gingeras, T.R. (2013). STAR: ultrafast universal RNA-seq aligner. Bioinformatics *29*, 15–21. https://doi.org/10.1093/bioinformatics/bts635.

107. Andrews, S. (2010). FastQC: A Quality Control Tool for High Throughput Sequence Data.

108. Bray, N.L., Pimentel, H., Melsted, P., and Pachter, L. (2016). Near-optimal probabilistic RNA-seq quantification. Nat. Biotechnol. *34*, 525–527. https://doi.org/10.1038/nbt.3519.

109. R Core Team (2021). R: A Language and Environment for Statistical Computing (R Foundation for Statistical Computing).

110. Wickham, H. (2016). ggplot2: Elegant Graphics for Data Analysis (Springer-Verlag).

111. Kolde, R. (2012). Pheatmap: Pretty Heatmaps. R Package. version 1.0. 12.

112. Korotkevich, G., Sukhov, V., Budin, N., Shpak, B., Artyomov, M.N., and Sergushichev, A. (2016). Fast gene set enrichment analysis. Preprint at Bioinformatics. https://doi.org/10.1101/060012.

113. Neuwirth, E. (2022). RColorBrewer *1*, 1–3.

114. Johnson, W.E., Li, C., and Rabinovic, A. (2007). Adjusting batch effects in microarray expression data using empirical Bayes methods. Biostatistics *8*, 118–127. https://doi.org/10.1093/biostatistics/kxj037.

115. Schneider, C.A., Rasband, W.S., and Eliceiri, K.W. (2012). NIH Image to ImageJ: 25 years of image analysis. Nat. Methods *9*, 671–675. https://doi.org/10.1038/nmeth.2089.

116. Lambert, S.A., Jolma, A., Campitelli, L.F., Das, P.K., Yin, Y., Albu, M., Chen, X., Taipale, J., Hughes, T.R., and Weirauch, M.T. (2018). The human transcription factors. Cell *172*, 650–665. https://doi.org/10.1016/j.cell.2018.01.029.

117. Michea, P., Noël, F., Zakine, E., Czerwinska, U., Sirven, P., Abouzid, O., Goudot, C., Scholer-Dahirel, A., Vincent-Salomon, A., Reyal, F., et al. (2018). Adjustment of dendritic cells to the breast-cancer microenvironment is subset specific. Nat. Immunol. *19*, 885–897. https://doi.org/10.1038/s41590-018-0145-8.

118. Soneson, C., Love, M.I., and Robinson, M.D. (2015). Differential analyses for RNA-seq: transcript-level estimates improve gene-level inferences. F1000Res. *4*, 1521. https://doi.org/10.12688/f1000research.7563.2.

119. Tang, Z., Kang, B., Li, C., Chen, T., and Zhang, Z. (2019). GEPIA2: an enhanced web server for large-scale expression profiling and interactive analysis. Nucleic Acids Res. *47*, W556–W560. https://doi.org/10.1093/nar/gkz430.

STAR★METHODS

KEY RESOURCES TABLE

REAGENT or RESOURCE	SOURCE	IDENTIFIER
Antibodies		
APC Mouse Anti-Human CD1a	BD Biosciences	Cat# 559775 RRID:AB_398669
FITC Mouse Anti-Human CD1a	BD Biosciences	Cat #555806 RRID:AB_396140
PE Mouse Anti-Human CD16	BD Biosciences	Cat # 347617 RRID:AB_400331
PE Mouse Anti-Human CD86	BD Biosciences	Cat # 555658 RRID:AB_396013
FITC Mouse Anti-Human CD80	BD Biosciences	Cat # 560926 RRID:AB_10565975
FITC Mouse Anti-Human HLA-DP,DQ,DR	BD Biosciences	Cat # 562008 RRID:AB_10897011
APC-Cy^{TM}7 Mouse Anti-Human HLA-DR	BD Biosciences	Cat # 335796 RRID:AB_399974
Purified Mouse Anti-Human CD1a	BD Biosciences	Cat#555805 RRID:AB_396139
Alexa Fluor® 488 AffiniPure Donkey Anti-Mouse IgG (H + L)	Jackson ImmunoResearch	Cat# 715545150 RRID: AB_2340846
Alexa Fluor® 594 AffiniPure Donkey Anti-Rat IgG (H + L)	Jackson ImmunoResearch	Cat# 712585153 RRID: AB_2340689
Purified Rat Anti Tubulin	Abcam	Cat# 6161 RRID: AB_305329
APC Mouse Anti-Human IFNγ	BD Biosciences	Cat# 554702 RRID:AB_398580
PE Mouse Anti-Human CD8	BD Biosciences	Cat# 557086 RRID:AB_396581
PerCP Mouse Anti-Human CD4	BD Biosciences	Cat# 550631 RRID:AB_393791
APC Mouse Anti-Human CD274 (PD-L1)	Biolegend	Cat# 374513 RRID:AB_2734441
PE Mouse Anti-Human CD207 (Langerin)	Biolegend	Cat# 352204 RRID:AB_10897451
PE Mouse Anti-Human FcεRI	Thermo Fisher	Cat# 12-5899-42, RRID:AB_10804885
Rabbit Anti-Phospho-p70 S6 kinase (Thr389)	Cell Signaling	Cat# 9205 RRID:AB_330944
Mouse Anti β-actin	Thermo Fisher	Cat# MA5-15739 RRID:AB_2537660
Co-Stimulatory Antibodies (CD28/CD49d) BD Fastimmune®	BD Biosciences	Cat# 347690 RRID:AB_647457
Peroxidase AffiniPure Goat Anti-Rabbit IgG (H + L)	Jackson ImmunoResearch	Cat# 111035144 RRID:AB_2307391
Peroxidase AffiniPure Goat Anti-Mouse IgG (H + L)	Jackson ImmunoResearch	Cat# 115035003 RRID:AB_10015289
Chemicals, peptides, and recombinant proteins		
eBioscience^{TM} CFSE	Invitrogen	Cat# 65-0850-84
DAPI Fluoromount-G®	Southern Biotech	Cat# 0100–20
Temsirolimus	Sigma-Aldrich	Cat# PZ0020
Temsirolimus	Cayman Chemical Company	Cat# 11590
Prostaglandin E2	Sigma-Aldrich	Cat# P0409
GW9662	Cayman Chemical Company	Cat# 70785
GW6471	Cayman Chemical Company	Cat# 11697
GSK3787	Cayman Chemical Company	Cat# 15219
Rosiglitazone	Cayman Chemical Company	Cat# 71740
Monensin – BD GolgiStop	BD Biosciences	Cat# 554724
CEF peptide pool - PepTivator® CEF MHC Class I Plus	Miltenyi Biotec	Cat# 130098426
M-CSF	Miltenyi Biotec	Cat# 130096493
GM-CSF	Miltenyi Biotec	Cat# 130093868
IL-4	Miltenyi Biotec	Cat# 130093924
TNFa	Miltenyi Biotec	Cat# 130094014
Bodipy FLC16 (Palmitic acid)	Thermo Fisher	Cat# D3821
pH Rhodo red zymosan particles	Thermo Fisher	Cat# P35364
OVA-DQ	Thermo Fisher	Cat# D12053

(*Continued on next page*)

Continued

REAGENT or RESOURCE	SOURCE	IDENTIFIER
Critical commercial assays		
Human IL-1β ELISA Set II	BD Biosciences	Cat# 557953
Human IL-6 ELISA Set	BD Biosciences	Cat# 555220
Human IL-8 ELISA Set	BD Biosciences	Cat# 555244
Human IL-10 ELISA Set	BD Biosciences	Cat# 555157
Human IL-12 (p70) ELISA Set	BD Biosciences	Cat# 555183
Human TNF ELISA Set	BD Biosciences	Cat# 555212
CBA Human Th1/Th2 Cytokine Kit II	BD Biosciences	Cat# 551809
RNeasy Plus Mini Kit	Qiagen	Cat# 74136
Deposited data		
RNA-seq Data	GEO	GSE210935
Software and algorithms		
DESeq2	(Love et al., 2014)[104]	https://bioconductor.org/packages/release/bioc/html/DESeq2.html
limma 3.16	(Ritchie et al., 2015)[105]	https://bioconductor.org/packages/release/bioc/html/limma.html
STAR 2.7.10a	(Dobin, A et al., 2013)[106]	https://doi.org/10.1093/bioinformatics/bts635
FastQC	(Andrews, 2010)[107]	https://www.bioinformatics.babraham.ac.uk/projects/fastqc/
kallisto 0.48.0	(Bray et al. 2016)[108]	https://pachterlab.github.io/kallisto/
R version 4.1.0	R Core Team (2021)[109]	https://www.R-project.org/
ggplot2	(Wickham et al. 2016)[110]	https://ggplot2.tidyverse.org
pheatmap 1.0.12	(Kolde,2019)[111]	https://CRAN.R-project.org/package=pheatmap
fgsea 1.22.0	(Korotkevich, G et al. 2016)[112]	https://bioconductor.org/packages/fgsea/
RColorBrewer 1.1–3	(Neuwirth E, 2022)[113]	http://colorbrewer2.org
ComBat	(Johnson et al. 2007)[114]	https://rdrr.io/bioc/sva/man/ComBat.html
FlowJo V10	FlowJo LLC	www.flowjo.com
ImageJ	(Schneider et al., 2012)[115]	https://ImageJ.nih.gov/ij/

RESOURCE AVAILABILITY

Lead contact

Further information and requests for resources and reagents should be directed to and will be fulfilled by the lead contact, Jorge Geffner Ph.D., jorgegeffner@gmail.com.

Data and code availability

- RNA-seq data reported in this paper is available in the GEO database: GSE210935.
- This paper does not report original code.
- Any additional information required to reanalyze the data reported in this paper is available from the lead contact upon request.

EXPERIMENTAL MODEL AND SUBJECT DETAILS

Human blood samples

The studies performed in this work have been reviewed and approved by the institutional review board and local ethical committee. Buffy coats from healthy donors, between 18 and 60 years old and a balanced female: male ratio, were obtained from Hospital de Clínicas "José de San Martín", Facultad de Medicina, Universidad de Buenos Aires. All human samples used in this study would have been obtained even if this study was not carried out, and were supplied without any personal identifiable information.

METHOD DETAILS

Cell isolation

PBMCs were isolated by centrifugation on Ficoll-Paque (GE Healthcare, Argentina). Monocytes were isolated from PBMCs by Percoll gradient centrifugation as described (Repnik et al., 2003) or by positive selection using anti-CD14-coated magnetic beads according to the manufacturer's instructions (Miltenyi). In all cases, monocyte purity was >85%. CD4+ T cells were isolated from heparinized blood samples by negative selection using RosetteSep immunodensity procedure (Cell Signaling Technologies) (purity >95%).

Cell culture

Experiments were performed using RPMI-1640 medium (Sigma-Aldrich, #R8758) supplemented with 50 UI/mL penicillin, 50 μg/mL streptomycin, and 10% heat-inactivated Fetal Bovine Serum (FBS, Sigma-Aldrich) or 7% human AB serum from healthy volunteers. M-CSF, GM-CSF, TNF- α, and IL-4 were obtained from Miltenyi Biotec.

Flow cytometry and cell sorting

The analysis was performed by using a BD FACSCanto cytometer and BD FACSDiva software. APC anti-CD1a (# 559775), FITC anti-CD1a (#555806), PE anti-CD16 (#347617) PE anti-CD86 (# 555658), FITC anti-CD80 (#560926), FITC anti-HLA-DR (#555811), APCCy7 anti-HLA-DR (#335796), PerCP anti-CD4(#550631), PE anti-CD8 (#557086), APC anti-IFN-γ (#554702), were obtained from BD Biosciences. APC anti-CD274 (PD-L1) (#374513), PE anti-CD207 (Langerin) (#144203) and Zombie NIR Fixable Viability Kit, were obtained from Biolegend. Sorting of $CD1a^{+}$ $CD16^{-}$ cells was performed using a BD FACSAria Fusion cytometer. PE anti human FcεRI alpha (# 12-5899-42) was obtained from Thermo Fisher.

Fatty acid uptake assay

Monocytes were cultured for 18 h under the specified experimental conditions. Afterward, 1μM of Bodipy FLC16 (Palmitic acid), Thermo Fisher (#D3821) was added to the cultures. Fatty acid uptake was then evaluated by FACS at 4 h by analyzing the fluorescence in the FL1 channel.

Phagocytosis assay

Mo-DCs were incubated for 2 h in the presence of zymosan fluorescent labeled particles (pH Rhodo red zymosan particles, Thermo Fisher, #P35364) at a concentration of 0.5 mg/mL. When exposed to the acidic pH of endolysosomal compartments, the dye becomes fluorescent, and thus enables the discrimination of intracellular vs extracellular particles. Cell fluorescence was analyzed either by FACS and by confocal microscopy after 30 min of adherence in polylysine-coated coverslips, and staining with anti CD1a. As a control, cells were also kept at 4°C in the presence of phRhodo Red zymosan particles to account for unspecific fluorescence uptake.

OVA-DQ processing assay

Mo-DCs were cultured for different times in the presence of OVA-DQ (Thermo Fisher, #D12053) at a concentration of 10 μg/mL. After proteolytic degradation, the compound fluoresces in the FL1 channel and is directly proportional to the quantity of degraded OVA. As a control, cells were also kept at 4°C in the presence of OVA-DQ to account for nonspecific fluorescence.

Reanalysis of microarray and scRNAseq datasets

Microarray datasets GSE40484 and GSE96703 were obtained from GEO. Normalized expression values were analyzed using RStudio 4.1.0 and the limma package (Ritchie et al., 2015)[105] (lmFiT function). Fold changes and p values between comparisons were calculated in a pairwise manner using donor as a blocking factor. Gene Set Enrichment Analysis was performed using the *fgsea* package and the KEGG gene sets. Plots were performed with *ggplot2*. (Tables S1 and S2). Single-cell RNAseq data were analyzed from (http://panmyeloid.cancer-pku.cn) (Cheng et al., 2021).[29] Dataset consists of batch-corrected gene expression data of myeloid cells from 15 different human tumors combined.

Quantitative Real-Time PCR (qPCR)

Cells were lysed and RNA was extracted using PureLink RNA Mini Kit. 100–200 ng of RNA were retrotranscribed into cDNA using Promega M-MLV reverse transcriptase in the presence of dNTPs and Random primers. qPCR was performed using SYBR Green PCR Master Mix (Applied Biosystems) and specific forward and reverse primers at a final concentration of 250 nM. Primer sequences used were:

FABP4_Fw: GGATGGAAAATCAACCACCA;
FABP4_Rv: GGAAGTGACGCCTTTCATGA;
ACTB_Fw: GGAAGTGACGCCTTTCATGA;
ACTB_Rv: CAGGAGGAGCAATGATCTTGATCT.

Cell lysates and immunoblots

Cells were washed in cold PBS and pellets were lysed in 4 x Laemmli sample buffer (Bio-Rad) with the addition of phosphatase (Merk) and protease inhibitor cocktails (Roche). Equal amounts of lysates were separated on 12% SDS-PAGE, blotted on PVDF transfer membrane (Thermo Fisher Scientific). Blots were revealed using Super Signal West Pico Chemiluminescent Substrate (Thermo Fisher Scientific). The intensity of the bands was quantified using the software ImageJ (National Institutes of Health). Anti-Phospho-p70 S6 kinase (Thr389) antibody (#9205, Cell Signaling) and Anti β-actin (#MA5-15739, Thermo Fisher Scientific- Invitrogen) were used as primary antibodies. HRP conjugated secondary antibodies were purchased from Jackson ImmunoResearch.

RNAseq library preparation

Cell pellets (200.000–500.000 cells) either from sorted CD1a^{+} CD16^{-} cells or from monocytes cultured for 8 h under different experimental conditions, were lysed for RNA extraction. Total RNA from cells was isolated using QIAGEN RNeasy Mini Kit according to the manufacturer's instructions. Briefly, the cells were lysed in Buffer RLT, supplemented with 1% b-mercaptoethanol. An equal volume of 70% ethanol was added to the lysate and transferred to the RNeasy spin column. After centrifugation, the flow through was discarded. This was followed by on-column DNase I treatment. 80 μL of DNase I mix (70 μL Buffer RDD with 10 μL DNase I) was added directly to the RNA spin column, incubated for 10 min at room temperature, and then washed. Finally, total RNA was eluted in 50 μL RNase-free water, and stored at −80°C. RNA-seq libraries were prepared with KAPA mRNA Hyperprep kit (Roche) according to manufacturer's instruction. First, poly An RNA was isolated from 300 ng total RNA using oligo-dT magnetic beads. Purified RNA was then fragmented at 85°C for 6 min, targeting fragments range 250–300bp. Fragmented RNA was reverse transcribed with an incubation of 25°C for 10 min, 42°C for 15 min and an inactivation step at 70°C for 15 min. This was followed by second strand synthesis and A-tailing at 16°C for 30 min and 62°C for 10 min. A-tailed, double stranded cDNA fragments were ligated with illumina unique dual indexed adapters (Illumina). Adapter-ligated DNA was purified using Ampure XP beads. This is followed by 10 cycles of PCR amplification. The final library was cleaned up using AMpure XP beads. Quantification of libraries were performed using real-time qPCR (Thermo Fisher). Sequencing was performed on Illumina NovaSeq platform generating paired end reads of 150bp.

RNAseq data analysis

FASTQ files were processed and aligned using *STAR* (Dobin et al., 2013) with hg38-assembly reference and NCBI RefSeq gtf from UCSC genome browseS4Dr data files. Analysis was performed using Rstudio v 1.4.1106, running R v. 4.1.0. *DESeq2* R package was used for the analysis of differentially expressed genes (Love et al., 2014), after filtering lowly expressed genes (<10 counts per row). For the differential expression analysis donor interindividual variability was considered a covariate and accounted for in the statistical comparisons. Genes were considered differentially expressed among comparisons when adjusted p value <0.1 (Benjamini and Hochberg method) using a Fold Change cutoff of 1.5 (Log2 0.58). *Enhancedvolcano* R package was used to produce the volcano plots. Heatmaps were generated using the *heatmap.2* and *pheatmap* packages. The rest of the plots were made using *ggplot2*. Gene set enrichment analysis was performed using *fgsea* package (Korotkevich et al., 2016). For the differential analysis of human transcription factors, the curated gene list was obtained from.[116] Normalized gene expression data can be interactively accessed at: https://ferra-uba-jax.shinyapps.io/shinnyapp/.

Publicly available gene expression data (RNAseq) from sorted peripheral blood cells were used for PCA analysis comparing *in vitro* generated Mo-DCs, CD14+ monocytes, cDC1, cDC2, pDCs and Axl + DCs. cDC1 and cDC2 data were obtained from GSE108174. CD14+ monocytes, pDCs and Axl + DCs data were obtained from GSE151073. Raw counts from all datasets were scaled and normalized (Log2 (CPM+1)). Genes with less than 1 Log2 (CPM+1) in more than 80 percent of the samples were excluded from the analysis. A total of 12,612 genes passed this filter. A significant batch effect was observed among datasets, and batch correction was performed using Combat.[114] Batch corrected expression data were used for PCA analysis. RNAseq data of tumor associated Macs and DCs from lobular breast cancer were obtained from PRJNA380940 (Michea et al. 2018).[117] FastQ files were pseudoaligned to the human reference Ensembl transcriptome GRCh38 using *Kallisto v.0.48.0*,[108] and raw count matrix was generated using *tximport*.[118] After normalization and scaling (Log2 (CPM+1)) of all datasets, genes with less than 1 Log2 (CPM +1) in more than 80 percent of the samples were excluded from the analysis. A total of 12,111 genes passed this filter and were used for downstream analysis. After batch correction, PCA was used to compare the transcriptomes of *in vitro* generated Mo-DCs with tumor-associated Macs and DCs. To analyze the correlation between the gene expression signature of GMTGW Mo-DCs and cancer progression in human tumors, we used the top 150 upregulated genes as input (Table S4) for the GEPIA2 http://gepia2.cancer-pku.cn/software, using the TCGA database.[119]

Fluorescence and confocal microscopy

Cells were recovered, washed with PBS, and resuspended in fresh RPMI medium followed by 30 min of adhesion on Poly-L-Lysine coated glass coverslips. The attached cells were washed with PBS and fixed with 4% PFA solution at 4°C for 15 min. Afterward, coverslips were treated for 10 min with glycin 0.1M in PBS solution to quench aldehyde group autofluorescence and blocked with 1% BSA solution in PBS. Coverslips were then incubated for 1 h at room temperature with purified mouse anti-human-CD1a (#555805, BD) in PBS 1% BSA (1:50 dilution). Coverslips were incubated for 15 min in BD Perm/Wash and then for 1 h at room temperature with rat anti-human tubulin (#6161, Abcam) in PBS 1% BSA (1:50 dilution). Coverslips were washed and incubated for 1 h at room temperature with donkey Alexa 488 anti-mouse IgG (1:500) and donkey Alexa 594 anti-rat IgG (1:500) (Jackson ImmunoResearch). The

coverslips mounted with DAPI-Fluoromount-G (SouthernBiotech) were examined under a confocal microscope (ZEISS LSM 900) using a Plan Apochromat 63 ×1.42 NA oil immersion objective.

Measurement of cytokines by ELISA

Cell culture supernatants from monocyte-derived cells were harvested and analyzed for the presence of IL-12(p70), IL-10, IL-1β, TNFα, IL-6, and IL8. Supernatants collected from the MLRs (mixed lymphocyte cultures) on day 6 of culture were analyzed for the presence of IFNγ, IL-2, IL-5, TNF-α, and IL-6. ELISA was performed with BD OptEIA sets according to the manufacturer's recommendations or using CBA Human Th1/Th2 Cytokine Kit II (BD).

Mixed lymphocyte reaction proliferation assays

Isolated CD4+ T cells were labeled with 5 μM CFSE (Molecular Probes, Invitrogen) in PBS for 5 min at 37°C. Cells were washed and plated (2×10^5/200 μL) in 96 well plates. Allogeneic monocyte-derived cells were counted and added to the lymphocyte cultures at a 1:4 antigen-presenting cell/CD4+T cell ratio. On day 6, cells were collected and CFSE dilution was assessed by flow cytometry. Quantification of absolute numbers of CD4+ T cells was determined by counting the number of T cells that diluted CFSE dye in the total recovered cell suspension.

Antigen-specific CD8 T cell activation assay

Following PBMC collection from buffy coats, monocytes were isolated and cultured ($1x10^6$/ml) for 6 days in RPMI medium supplemented with 7% heat-inactivated human AB serum, in the presence of GM-CSF (50 ng/mL) + IL-4 (30 ng/mL) or GM-CSF (50 ng/mL) + Temsirolimus (50 nM) + GW9662 (10 μM), to induce their differentiation into Mo-DCs. A fraction of the PBMCs was frozen into two vials containing 20×10^6 cells for later use in the experiment. Mo-DCs were harvested and cultured (1×10^6/ml) in RPMI +7% heat-inactivated AB serum for 18 h in the presence of LPS (10 ng/mL), with or without the addition of CEF peptide pool (10 μg/mL) (Miltenyi Biotec #130-098-426). CEF peptide pool contains 32 MHC-I restricted peptides of 8–12 aa in length from human cytomegalovirus (HCMV), Epstein-Barr virus (EBV), and Influenza virus. Most individuals have a detectable proportion of antigen-experienced memory CD8 T cells that specifically recognize some of these peptides. For each experiment, autologous PBMCs were thawed the same day of Mo-DC harvest, and cultured for 18 h (1×10^6/ml) in RPMI 7% AB serum before the coculture with peptide-pulsed Mo-DCs. PBMCs were labeled with CFSE 5 μM in PBS for 5 min, washed again, and cocultured with mock or peptide-pulsed Mo-DCs, in 12 well dishes: $2x10^6$ PBMCs and 1×10^6 Mo-DCs in 3 mL final volume. After 7 days of culture, half of the culture media was replaced every 2–3 days with fresh RPMI medium supplemented with 7% heat-inactivated human AB serum. The total duration of the coculture was 12 days. In order to analyze the extent of the expansion of antigen-reactive $CD8^+$ T cells, lymphocytes were harvested, washed, and rechallenged or not with CEF peptides (1 μg/mL), in the presence of autologous CFSE-labeled PBMCs (thawed the same day of the assay) to serve as antigen-presenting cells. $5x10^5$ expanded T lymphocytes were cocultured with $5x10^5$ autologous PBMCs in round bottom 96 well plates. Cells were then cultured in the presence or absence of CEF peptides, with the addition of CD28/CD49d (1 μg/mL) costimulatory antibodies (BD Fastimmune,#347690). One hour after the beginning of the culture, monensin (BD GolgiStop) (1:1500) was added to each well. The intracellular expression of IFN-γ in $CD8^+$ T cells was then analyzed by FACS. Because part of the CFSE labeling is partially lost through prolonged culture, by using this strategy we were able to distinguish freshly added PBMCs (which only served a technical purpose in the assay) from lymphocytes coming from the coculture with Mo-DCs (either having engaged proliferation or not). A diagram of the process is presented in Figure S5A.

Chemicals

Temsirolimus (#11590), GW9662 (#70785), GW6471 (#11697), GSK3787 (#15219), and Rosiglitazone (#71740) were purchased from Cayman Chemical Company. PGE2 was purchased from Sigma Aldrich (#P0409). LPS from Escherichia coli O111:B4 (#L4391).

QUANTIFICATION AND STATISTICAL ANALYSIS

When comparing two groups, normally distributed data were analyzed using t-tests, and skewed data were analyzed by Wilcoxon test. For 3 or more groups, One way-ANOVA or Kruskal–Wallis test was used. Data analysis was performed using GraphPad Prism software version 8 (GraphPad, San Diego, CA, USA). Differences were considered to be statistically significant at p-value <0.05.